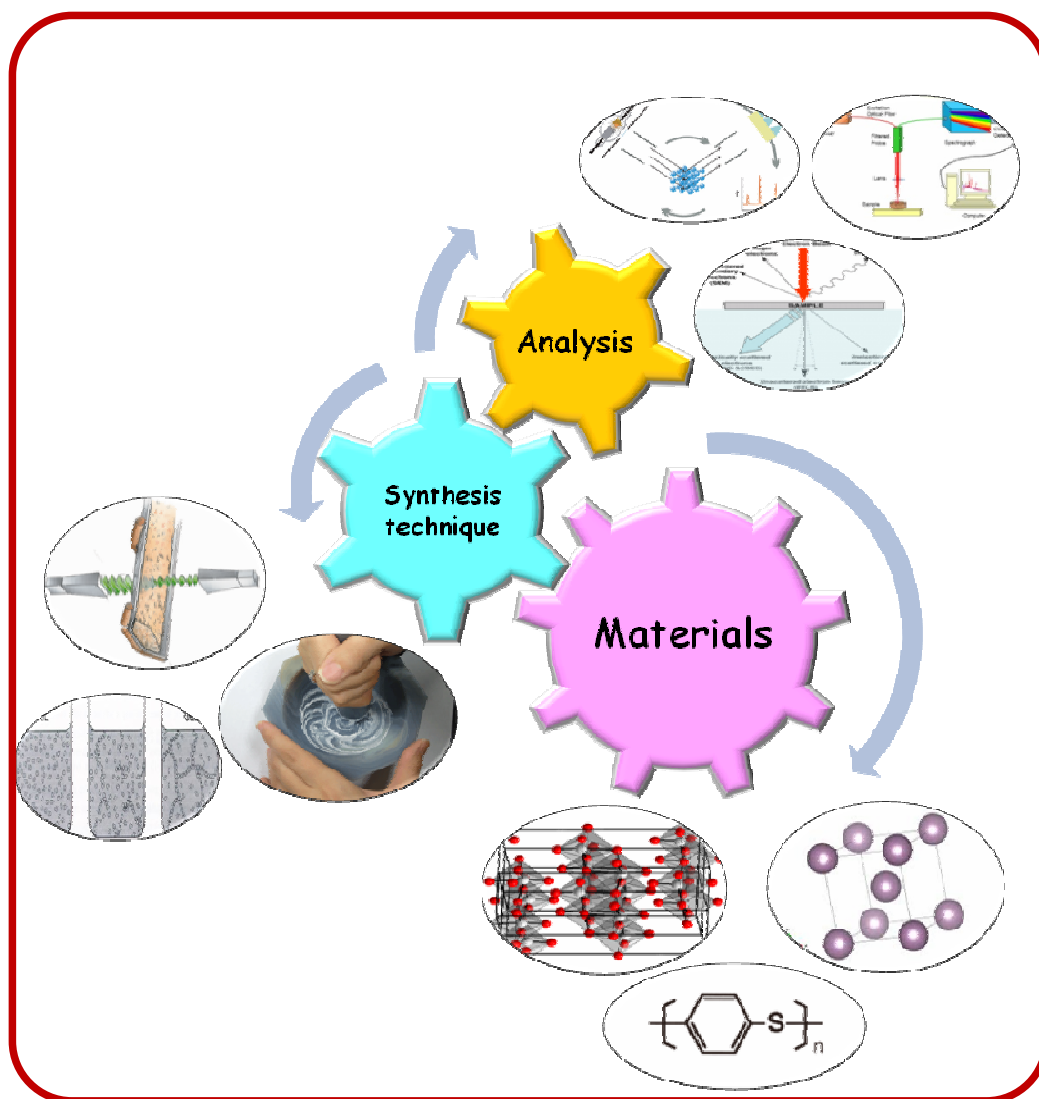


Chapter 2

Literature Survey



“Science cannot progress without reliable and accurate measurement of what it is you are trying to study. The key is measurement, simple as that.”

- Robert D. Hare

2.1 Introduction

As mentioned in the summary of chapter 1, advancements in the field of synthesis of nanomaterials are still governed by certain prominent yet unfulfilled challenges. Some of the **key** challenges are:

- (i) *Facile, economical and green synthesis methods*
- (ii) *Large-scale synthesis of nanoparticles having precise control over the morphology of the synthesized products*
- (iii) *Synthesis of metal-metal oxide-polymer nanocomposites to realize technological applications*
- (iv) *Swift reaction rates*
- (v) *Synthesis of nanostructures flaunting complex and hierarchical shapes with precise control over the size and shapes of these structures.*

Nevertheless, it is not possible to counter all the challenges following only one kind of synthesis protocol and demand synergistic approaches. To tackle these challenges with respect to chemical synthesis, an extensive literature survey was carried out for the present work. Prior knowledge of various synthesis techniques that are available for the synthesis of nanostructures of different sizes and shapes is the keystone for nanomaterials development aspects. Synthesis of nanostructures in various forms can be broadly classified into three main types based on the process employed for the synthesis viz (i) Physical techniques, (ii) Chemical techniques and (iii) Biomimetic/biological techniques. Excellent reviews are available pertaining to these synthesis techniques [1]. With regards to few synthesis challenges, initial success was achieved in physical synthesis techniques like mechanical milling and vapour phase routes. Various vapour phase synthesis techniques have been reported [2] which make it possible to synthesize materials on large scale. Later, it was found out that most of these techniques were triumphant at the synthesis of certain nanomaterials, especially, nanomaterials of various oxides but the success rate for metals and metals sulfides are not very high. In addition, many of these processes lacked in energy and cost effectiveness. To overcome these problems, various chemical techniques have been proposed which can tackle most of the problems associated with synthesis of nanomaterials [3]. Most of the chemical routes are cost effective, facile and can have precise control over the morphologies of nanostructures. It may still be noted that any single chemical synthesis technique also is not capable of solving all the problems posed above. For example, some of these techniques employ precursors and solvents for the synthesis of naomaterials and can create an issue of contamination of final nanoscale products

with these intermediate products and unreacted precursors. In many of the techniques, the reaction time can be very high (hours to days). Another problem with few techniques where the reaction takes place at low temperature is the lack of crystallinity.

In the present work, only wet chemistry route has been followed for the synthesis of nanostructured materials. There are plenty of wet chemistry routes available and have also been reported in the form of review articles [1, 4]. In order to tender the brevity, only the techniques which have been employed in the present research work for nanomaterial synthesis and their characterization have been discussed in this chapter 2.

Related standard publications from national & international journals, standard patents, and standard books or websites were referred for the sake of completeness of the review data generation. Based on this literature survey, we could arrive at the motivation and scope of this dissertation and create the strategy for synthesis, characterization, and applications of the selected nanomaterials which have been defined in the last section (section 2.5) of this chapter.

2.2 Wet Chemistry Routes of Nanosynthesis

Typically, chemical synthesis techniques bank upon nucleation and growth that are simultaneously accompanied by the chemical reactions like decomposition, recombination, oxidation, and reduction, etc. Each synthesis method is governed by its rate of nucleation and growth. Thus, structural and morphological aspects of the synthesized products depend on the major factors namely the type of chemical reaction, pH of the reaction, environment (a type of solvent, reactants, etc), temperature, etc. A brief review of different chemical techniques used for the synthesis of nanomaterials in the present case, i.e. a) conventional hydro/solvothermal route, b) microwave assisted solvothermal route, c) solid - solid route and d) sol-gel route is provided in this section.

2. 2.1 Hydro/solvothermal technique

Among the galaxy of synthesis techniques available, hydro/solvothermal techniques are profoundly essential shining twin stars for advanced materials processing, especially, owing to their advantages in the synthesis of nanostructured materials for a wide variety of technological applications in electronics, optoelectronics, catalysis, ceramics, magnetic data storage, biomedical, biophotonics, etc.

In an autoclave (bomb, sealed vessel, etc.), an increase in autogenous pressure resulting from heating brings solvents to temperatures well above

their boiling points. Performing a chemical reaction under such conditions is referred to as solvothermal processing or, in the case of water as a solvent, hydrothermal processing.

Water is said to be supercritical above the temperature and pressure of 374°C and 218 atm (the critical point for water). Supercritical fluids exhibit characteristics of both a liquid and gas, namely, the interfaces of solids and supercritical fluids lack surface tension, yet supercritical fluids exhibit high viscosities and possess the ability to readily dissolve chemical compounds that would otherwise display very low solubilities under ambient conditions. Few solvothermal processes indeed contain solvents which work under supercritical conditions. Nevertheless, most others simply rely on the increased solubility and reactivity of metal salts and complexes at elevated temperatures and pressures without bringing the solvent to its critical point. Under most circumstances, hydro/solvothermal processing facilitates many inorganic materials to be produced at temperatures substantially below those required by traditional wet chemistry routes. Additionally, the products of hydro/solvothermal reactions are usually crystalline and do not require post-annealing treatments unlike the cases of co-precipitation and sol-gel methods (which also occur at substantially reduced reaction temperatures).

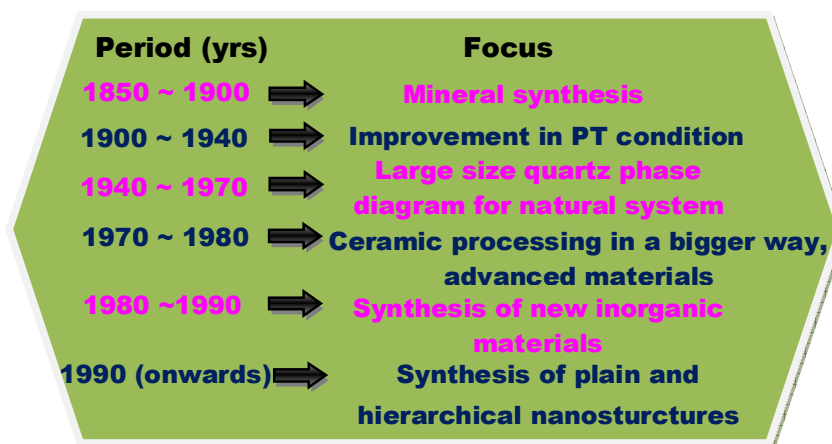


Figure 2.1 History of hydrothermal synthesis.

The definition of the word hydrothermal has undergone several changes from the original Greek meaning of the phrase ‘hydros’ meaning water and ‘thermos’ meaning heat. Historically, the origin of the term ‘hydrothermal’ can be traced to geology and was first popularized by the British geologist, Sir Roderick Murchison (1792-1871). He used this term to describe the action of water at elevated temperature and pressure which brings about an alteration in the

earth's crust leading to the formation of various rocks and minerals. A brief history regarding the hydrothermal processing is provided in figure 2.1. It is well known that the largest single crystal formed in nature (beryl crystal of >1000 g) and some of the large quantity of single crystals created by man in one experimental run (quartz crystals of several thousand of grams) are both of hydrothermal origin [5].

In general, hydrothermal processing is defined as any heterogeneous reaction (utilizing aqueous solvents or mineralizers) under high pressure and temperature conditions to dissolve and recrystallize (recover) materials that are relatively insoluble under ordinary conditions. Recently, Byrappa and Yoshimura defined hydrothermal as any heterogeneous chemical reaction in the presence of a solvent (whether aqueous or non-aqueous) above the room temperature and at a pressure greater than 1 atm in a closed system [5]. However, there is still some confusion about the very usage of the term hydrothermal and solvothermal. It may be noted that both these terms go hand in hand and their characteristics are strikingly similar. To avoid the repetition, the term hydro/solvothermal has been used to describe the phenomena of hydrothermal and solvothermal reactions.

Important parameters for hydro/solvothermal technology

The major parameters of hydrothermal synthesis which determine the process kinetics as well as the properties of resulting products are:

- a) *initial pH of the medium,*
- b) *time duration of the reaction,*
- c) *synthesis temperature,*
- d) *pressure in the system,*
- e) *volume of the solvents and*
- f) *directing agents*

Most of these parameters are governed by the 'ideal gas law' which is given as:

$$PV = nRT \text{ ----- [2.1]}$$

where, P - pressure of the system

V - volume of the system

n - amount of substance of system (also known as the number of moles)

R - ideal or universal system constant, equal to the product of the Boltzmann constant and the Avogadro constant.

T - temperature of the system.

On the basis of these parameters, the morphology of the particles or materials can be suitably tuned.

This synthesis method is useful to carry out large-scale production of micro to nano size particles. To accomplish synthetic reaction, adequate chemical precursors are dissolved in water and placed in steel or any vessel which can withstand high temperature typically up to 2000 °C and high pressure about 0.01 GPa. Typically, hydro/solvothermal synthesis is carried out in steel pressure vessels called 'autoclaves' or 'bombs' with or without Teflon liners under controlled temperature and/or pressure with the reaction in polar or non-polar solvents as shown in figure 2.2. The temperature can be set above the boiling point of the solvent, attaining the pressure of vapor saturation. The temperature, as well as the amount of added solvent mainly decide the internal pressure produced in the autoclave. For the present work, Teflon-lined stainless steel autoclave as shown in figure 2.2 (B) has been employed. This technique is useful to obtain novel plain and hierarchical nanostructured particles. Particularly, this technique is important in the case of difficulty of dissolving the precursor at low/ordinary temperatures. This technique is also beneficial when there is a need to grow nanoparticles if the material has a high vapour pressure near its melting point or crystalline phases are not stable at the melting point. It can also be used to prepare many geometries including thin films, bulk powders, single crystals, and nanocrystals.

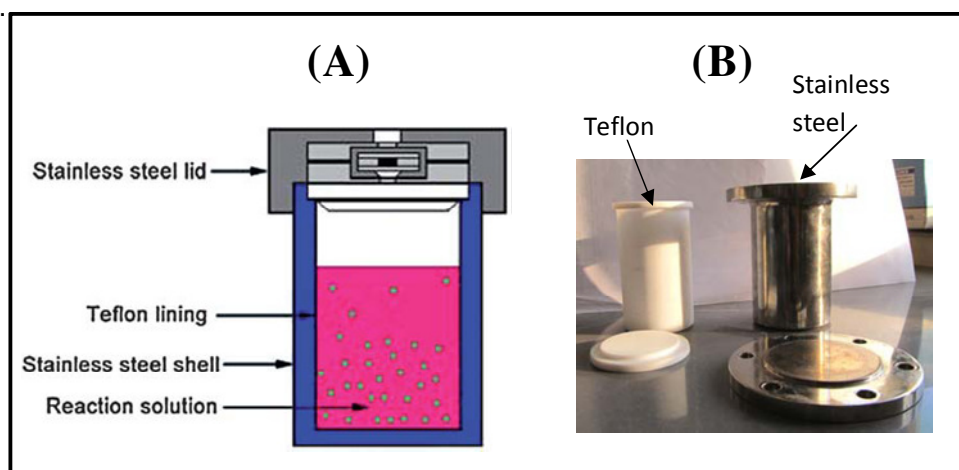


Figure 2.2 (A) Schematic of a Teflon-lined, stainless autoclave and (B) the actual digital photograph of stainless steel autoclave with Teflon liner typically used in this dissertation

In addition, the morphology (sphere (3D), rod (2D), or wire (1D)) of the formed crystals can be resourcefully controlled by manipulating the solvent

supersaturation, chemical of interest concentration, and kinetic control. Various oxide [6], sulfide [7], nitride [8] nanoparticles have been synthesized by the hydro/solvothermal technique.

Advantages of hydro/solvothermal technology

The advantages offered by hydro/solvothermal technique are enlisted below:

- *Thermodynamically stable and metastable states (including novel materials) can be effortlessly prepared.*
- *Versatile, economical, environment friendly and facile.*
- *No post-heat treatment which reduces aggregation.*
- *No milling process which reduces impurity due to contamination.*
- *Controllable particle size & shape*
- *Relatively cheap raw material can be used*
- *Preparation of the hybrid materials is possible*
- *Comparatively reduced reaction time by at least 2-3 orders of magnitude as compared to the most wet chemistry routes.*

Additionally, this technique can be coupled with other chemical routes or energies like microwave, ultrasonic, mechanical and electrochemical to fine tune hydro/solvothermal reaction kinetics. Under these circumstances, an attempt has also been made to explore microwave assisted hydro/solvothermal synthesis of nanostructures in the present dissertation work. To orient the subject matter in the proper perspective, a brief introduction about microwave assisted hydro/solvothermal synthesis of nanostructures has been provided in section 2.2.2.

2.2.2 Microwave assisted solvothermal synthesis

Despite numerous advantages offered by hydro/solvothermal technique corresponding to nanomaterials synthesis, relatively longer reaction times (in hours) is a major drawback. Improvement in the thermodynamical conditions by an enhancement in the reaction kinetics of the reaction can overcome this drawback. One significant way to achieve this is the employment of microwave energy in hydro/solvothermal reactions. This novel method is now popular as microwave assisted solvothermal route for the synthesis of nanomaterials of various morphologies [9, 10]. This approach is exploited in the present study for the synthesis of metal sulfide nanostructure namely, molybdenum disulfide (MoS_2). A brief discussion on the philosophy of microwave assisted synthesis of nanomaterials is provided in the proceeding portion of this section.

Introduction to Microwaves

Microwaves constitute the fraction of the electromagnetic spectrum with corresponding frequencies between 300 MHz and 300 GHz (wavelengths

~1mm - 1m). Within this broad range of the electromagnetic spectrum, different frequency bands are allocated for cellular phones, radar, and television satellite communications. For microwave heating, 0.915 and 2.45 GHz are the only two frequencies which have been conferred by the Federal Communications Commission (FCC) for industrial, scientific, and medical (ISM) purposes. Figure 2.3 displays the electromagnetic spectrum including the microwave region. It also shows the different regions of the microwave spectrum which are allowed for utilization in commercial applications.

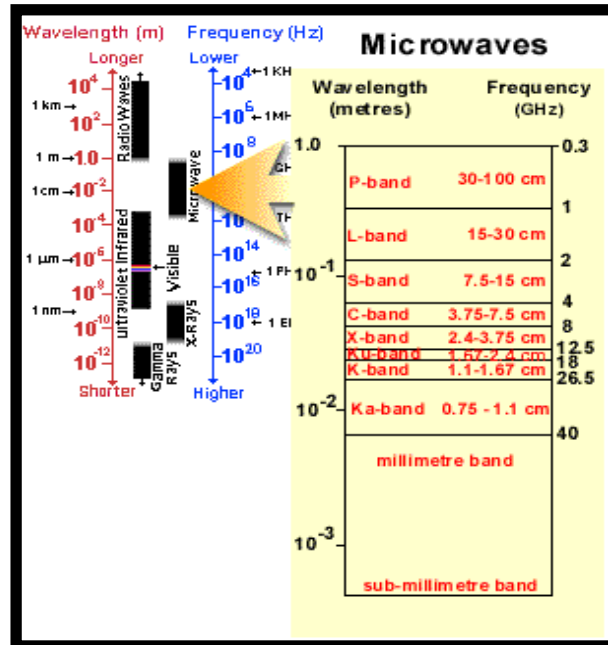


Figure 2.3 Electromagnetic spectrum and frequencies used in microwave processing [11].

Advantages of microwaves heating

Microwaves exhibit several advantageous characteristics that are absent in conventional processing of materials such as:

- ✚ Penetrating radiation;
- ✚ Controllable electric field distributions;
- ✚ Rapid heating (Please refer to figure 2.5);
- ✚ Selective heating of materials through differential absorption;
- ✚ Self-limiting reactions;
- ✚ No direct contact between the energy source and the reacting chemicals (energy efficient).

Opportunities and benefits provided by these characteristics, either singly or in combination, are not available from conventional heating or processing methods.

Thus, microwave heating lends alternatives for the processing of a wide variety of materials, including rubber, polymers, ceramics, composites, minerals, soils, wastes, chemicals, and powders. In this scenario, it is imperative to understand the phenomenon behind microwave heating as provided below.

Acceleration of charge, especially, electrons in the electromagnetic field leads to the production of electromagnetic radiation. High power and frequencies required for microwave heating are realized using vacuum tubes in most microwave sources. Magnetrons, traveling wave tubes, and klystrons are examples of some vacuum tubes that have been used for microwave heating. Among them, magnetron tubes used in home microwave ovens (also known as 'cooker magnetron') are efficient and reliable [12]. Magnetron tubes use resonant structures to generate the electromagnetic field, and therefore, are only capable of generating a fixed frequency electromagnetic field. In the present work, household microwave oven containing such magnetron is used for carrying out part of the synthesis of metal sulfide nanostructures. Concerning their interaction with microwaves in general, materials are categorized into:

- (i) **Microwave reflectors**, which are bulk metals and alloys, such as brass, and are used in making microwave guides;
- (ii) **Microwave transmitters**, which are transparent to microwaves. Such materials include fused quartz, zircon, several glasses, and ceramics (not containing any transition element), Teflon, etc. They are employed for making cookware and containers for carrying out chemical reactions in microwaves; and
- (iii) **Microwave absorbers**, which comprise the most important class of materials for microwave synthesis. They absorb the energy from the microwave field and get heated up very rapidly [13]. Water, ethanol, ethylenediamine are few examples of such materials.

Based on this, microwave furnaces are composed of *three* major components: the source, the transmission lines, and the applicator. The microwave source generates the electromagnetic radiation, and the transmission lines (reflector) deliver the electromagnetic energy from the source to the applicator. In the applicator, the energy is either absorbed or reflected by the material.

Two specific mechanisms of interaction between microwaves and materials absorbing microwave are [14]: (1) dipole interactions and (2) ionic conduction. Both mechanisms are governed by effective coupling between

components of the target material and the rapidly oscillating electrical field of the microwaves. Dipole interactions are dominating in the case of polar molecules. The polar ends of a molecule tend to align themselves and oscillate in cohesion with the oscillating electrical field of the microwaves (figure 2.4a). Due to the time lag (figure 2.4a), collisions and friction between the moving molecules result in heating. Broadly, the more polar a molecule, the more effectively it will couple with the microwave field. Ionic conduction is slightly different from dipole interactions. In this case, ions in solution do not have a dipole moment. Rather, they constitute charged species that are distributed and have a tendency to couple with the oscillating electrical field of the microwaves (figure 2.4b). The effectiveness or rate of microwave heating of an ionic solution is a function of the concentration of ions in solution.

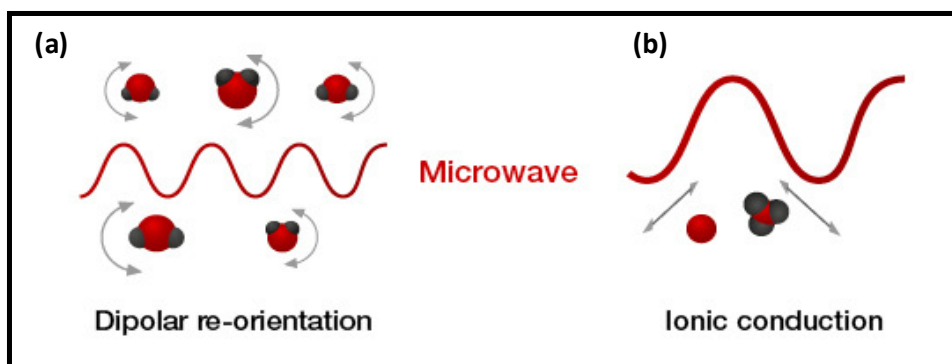


Figure 2.4 Mechanism of microwave heating a) dipole reorientation and b) ionic conduction [15].

During dielectric heating, the interaction of dielectric materials through electric dipoles with applied electric field of microwaves leads to heating effect [13]. Basically, significant factor for microwave heating is the reorientation dynamics of the dipoles in the applied alternating field. Phase lag in the reorientation emerges when the dipolar reorientation is unable to promptly respond to the frequency of the alternating electric field of the microwaves. As a consequence, polarization current arises which is in phase with the applied field. If the phase lag, field strength, and current are denoted by δ , E and I respectively, then the component of the in-phase current is $I \sin \delta$ (since E and I are 90° out of phase in an ideal dielectric) which culminates into resistive heating of the medium. In this regard,

$$\sin \delta \approx \tan \delta = \epsilon'' / \epsilon' \text{ ----- [2.2]}$$

which is the energy dissipation factor or loss tangent and can be considered as a convenient measure of the heating effect which occurs in an applied field (where ϵ' and ϵ'' are the real and imaginary parts of the dielectric constant). In materials such as liquids, the dipoles rotate freely, and the rotational frequency of the dipole determines the dissipation of energy from the applied field. If the dipolar relaxation is characterized by a single relaxation time τ and ω is the frequency of the applied field (such as of the microwaves), then the relations between dielectric quantities and the frequency are represented by the Debye equations 2.3 & 2.4:

$$\epsilon' = \epsilon_{\infty} + \frac{\epsilon_s - \epsilon_{\infty}}{1 + \tau^2 \omega^2} \quad \dots\dots\dots [2.3]$$

$$\epsilon'' = \frac{\epsilon_s - \epsilon_{\infty}}{1 + \tau^2 \omega^2} \quad \dots\dots\dots [2.4]$$

where, ϵ_s and ϵ_{∞} are the zero frequency and infinite frequency dielectric constants, respectively. Thus, ϵ'' varies with frequency giving rise to characteristic peak at $\omega\tau = 1$ or $\omega = 1/\tau$. For water at 20 °C, the value of the relaxation peak frequency is about 18 GHz and ϵ'' is quite significant at 2.45 GHz. Owing to this, there is a rapid dissipation of energy and hence heating of water in commercial ovens operating at 2.45 GHz. The microwave power dissipation per unit volume in a material, P , is dependent upon the total current σ and the square of the electric field E in the sample (equations 2.5 and 2.6):

$$P = \sigma |E|^2 = (\omega \epsilon_0 \epsilon'') |E|^2 \quad \dots\dots\dots [2.5]$$

or, in terms of ϵ' :

$$P = (\omega \epsilon_0 \epsilon' \tan \delta) |E|^2 \quad \dots\dots\dots [2.6]$$

In conjunction with the Debye relations (equations 2.3 and 2.4), P can be written as:

$$P = \frac{\epsilon_0 (\epsilon_s - \epsilon_{\infty}) \tau^2 \omega^2}{1 + \tau^2 \omega^2} |E|^2 \quad \dots\dots\dots [2.7]$$

A better understanding of physical properties of the materials can be used to predict their behavior in a microwave field. Dissipation factor, often called the loss tangent is one such important physical parameter which has to be calculated. The dissipation factor is the ratio of the dielectric loss (loss factor) to the dielectric constant. It may be noted that the dielectric loss is a measure of how well a material absorbs the electromagnetic energy to which it is exposed. Additionally, the dielectric constant is a measure of the polarizability of material, essentially how strongly it resists the movement of either polar molecules or

ionic species in the material. **Both the dielectric loss tangent ($\tan \delta$) and the dielectric constant (ϵ) are the most significant measurable properties with respect to the heating of materials via microwave radiation.**

Another significant parameter is penetration depth, D , which is the distance in the direction of penetration at which the incident power is reduced to half of its initial value (equation 2.8):

$$D = \frac{3\lambda_0}{8.686 \pi \tan \delta (\epsilon')^{1/2}} \quad \text{-----[2.8]}$$

where, λ_0 is the wavelength of the microwaves. The expression for the microwave penetration depth reveals that for most materials, D is significantly high and, therefore, microwave power dissipation is relatively uniform throughout the material as long as the sample sizes are not large. This transpires an important feature of microwave heating, namely, volumetric heating, which results in a temperature profile exhibiting a decreasing slope towards the geometrical borders of the sample in a manner opposite to that found in conventional heating. The situation is explained in figure 2.5

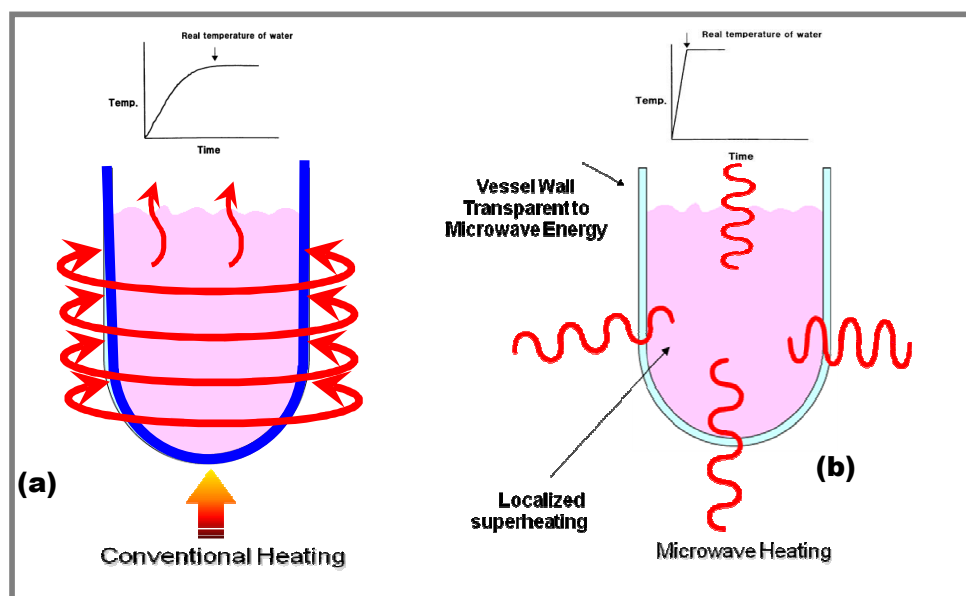


Figure 2.5 Increase of temperature with time and heating effect in (a) conventional-hydrothermal and (b) microwave-hydrothermal routes [16].

These selective interactions mean that microwave dielectric heating is an ideal method for accelerating chemical reactions under increased pressure conditions. For the most part, the synthetic methods utilize conventional convective heating due to the need for high-temperature initiated nucleation followed by controlled precursor addition to the reaction to achieve consistent growth. Conventional thermal techniques rely on conduction via blackbody

radiation to drive the reaction. The reaction vessel acts as an intermediary for energy transfer from the heating mantle to the solvent and finally to the reactant molecules (figure 2.5a). Such situation causes sharp thermal gradients throughout the bulk solution and inefficient, non-uniform reaction conditions (with higher reaction times). This is a common problem encountered in chemical scale-up and is made more problematic in nanomaterials where uniform nucleation and growth rates are critical to material quality. New approaches such as microwave heating for synthesis have been sought particularly for controlled growth. Specifically, the containment materials for a microwave assisted chemical reaction are chosen such that the microwave energy passes through the walls of the vessel and heats only the reactants (figure 2.5b). It is possible to increase the temperature of a reaction in common organic solvents up to 100 °C above the conventional boiling point of the solvent using quite a simple apparatus based either on transparent plastics (e.g. Teflon). For example, ethanol with a conventional boiling point of 79 °C can be raised rapidly to temperatures of 164 °C and a pressure of 12 atmospheres via microwave dielectric heating in a closed vessel. A thousand-fold acceleration of the reaction rate for the reactions that are carried out in this solvent can be achieved at such higher temperature [17].

Salient Aspects of Microwave Dielectric Heating:

1. Polar solvents are suitable candidates as solvents for microwave dielectric heating experiments owing to a permanent dipole moment, which in turn, dominates relaxation processes in the microwave region.
2. Even when the relaxation time is one or two orders of magnitude different from that which corresponds to the microwave frequency operating in the cavity, then the solvent is still capable of acting as an effective medium for dielectric heating because its loss tangent ($\tan \delta$) is sufficiently large. Typically, solvents with $\tan \delta \geq 0.1$ are suitable candidates for microwave dielectric heating experiments. Dielectric constant and dielectric loss tangent values obtained for some common solvents are enlisted in Table 2.1.
3. The relaxation time of a solvent is inversely dependent on the temperature. Therefore, an organic solvent with a relaxation time greater than around 65 picoseconds (ps) i.e. corresponding to 2.45 GHz, will have a loss tangent which increases with temperature. As the temperature increases as a result of microwave dielectric heating, the loss tangent increases and the solvent converts more of the microwave

energy into thermal energy consequently leading to rise in the heating rate. The resulting phenomenon is described as thermal runaway. It is not surprising that many organic solvents superheat in a microwave cavity as the majority of organic solvents have relaxation times ≥ 65 ps (in some cases it is larger than 1000 ps).

Solvent	Dielectric constant	$\tan \delta$
DI Water	76-78 @1MHz	0.005 @ 1MHz 0.157@ 3 GHz
Diethylene triamine (DETA)	12 @ 1KHz	-----
Ethylene glycol (EG)	41 @ 1MHz 12 @ 3 GHz	-0.003 @ 1MHz 0.1@ 3 GHz
Ethanol	24.5 @ 1MHz 6.5 @ 3 GHz	0.09 @ 1MHz 0.25@ 3 GHz

Table 2.1 Dielectric constant and $\tan \delta$ values of different solvents.

- Usually, high heating rates for the whole mixture can be attained by the addition of small amounts of a polar solvent with a large loss tangent. The energy transfer between the polar molecules coupling with the microwaves and the majority non-polar solvent is rapid and thus provides an effective mechanism for introducing non-polar solvents as coupling agents into a microwave cavity leading to the increased reaction kinetics.
- The addition of salts to solvents increases their conductivities imparting a dramatic influence on their heating rates.

Applications of microwave heating in nanomaterials synthesis

The most common and widely used application of microwave is in household cooking. In industry, microwave processing is used for sintering as well as in chemical synthesis [18]. The microwave-assisted route is yet another novel method of synthesis [19] and is a very rapidly developing area of research. Nowadays, microwave processing is also exploited for the synthesis of novel nanomaterials. In this context, microwave assisted synthesis techniques are not entirely new techniques of synthesis but are the modifications made to the existing techniques owing to the advantages of the microwave process/heating. By judicious choice of the solvents, passivating ligands and reactants, the nanomaterial precursors can be selectively heated preferentially with regards to

the solvent or passivating ligand. A succinct summary of the progress in nanomaterials synthesis using this route has been provided in Table 2.2.

Sr. No	Nanomaterials	Morphology	Reference
1.	CdSe, PbSe, and Cu _{2-x} Se,	Irregular, spherical, aggregated	[20]
2.	CdS	Nanosheets & spherical particles	[21]
3.	SnO ₂	Platelet-like shaped particle, pseudo spherical	[22]
4.	TiO ₂	Nanostructure spherical crystals	[23]
5.	Fe ₃ O ₄ and α-Fe ₂ O ₃	Irregular shapes and a few have the hexagonal	[24]
6.	CeO ₂	Rod-like, sphere-like nanoparticle	[25]
7.	ZnS	Nanostructures	[26]
8.	ZnO	Nanoparticles	[27]
9.	Ag, Au, Pt, and AuPd	Single crystalline polygonal plates, sheets, rods, wires, tubes, and dendrites	[28]
10.	MgO	Nanocrystalline particles	[29]
11.	Co ₃ O ₄ -graphene	Sheet-on-sheet nanocomposite	[30]

Table 2.2 Typical examples of microwave assisted nanomaterials synthesis.

In a nutshell, the microwave processing of materials provides:

- new approaches to improve the physical properties of the materials;
- alternatives for processing of nanomaterials that are hard to process;
- reduction of the environmental impact of materials processing;
- economic advantages through the saving of energy, space, and time; and
- an opportunity to produce nanomaterials with vivid morpho-structures.

Riding on above discussions on the microwave processing, we explored the synthesis of nanostructures of metal sulfide viz. molybdenum disulfide using

novel microwave assisted solvothermal technique which is an advanced version of already existing solvothermal synthesis technique. It may be noted that ours was the first attempt towards microwave assisted synthesis of molybdenum disulfide nanostructures.

Despite all such advantages, conventional as well as microwave assisted solvothermal routes suffer from two main disadvantages namely, extensive use of solvents and low production scale. Herein, an effort has been made to overcome these disadvantages using a novel solid state route which has been described in the section 2.2.3 in this chapter.

2.2.3 Solid state route

Historically, it has been assumed that chemical reactions can only occur through the intervention of solution media (Aristotle's Principle) to form molecular species [31]. In respect of this, most of the traditional chemical reactions are being carried out in the presence of solvents solution. In the literature, solid state reactions have not been mentioned in details. In the past, it was the oldest and most common method of preparing multicomponent solid materials [32, 33]. Over many years, solid state reactions have mostly been confined to refractory ceramics, especially ferrites [34] and process like ball milling. However, knowledge base generated has not been percolated to other disciplines such as nanomaterials synthesis.

A solid state reaction also called a dry media reaction or a solvent-less reaction, is a chemical reaction which is characterized by the absence of solvents. In typical chemical reaction, the reactants are placed in a solvent prior to the reaction. These reactants under the preset experimental conditions react to produce a new substance. After the completion of the reaction, the new product has to be extracted from the solvent using techniques such as centrifugation and drying. In a solid-state reaction, however, the reactants are allowed to react chemically without the presence of a solvent. Eliminating the requirement of solvent from the reaction ensures that a solid state reaction generates more product than a regular chemical reaction. It also is an environmentally friendly route. Since there is no solvent involved, there is no waste of time and energy to eliminate it at the end of the reaction. Also, some solvents are not good for environments, and their use should be avoided.

Solid-state reaction consists of reaction of the precursor materials in the solid state at elevated temperature involving repetitive operations of grinding, pelletizing and heating of the reacting materials to accomplish the reaction till the phase purity is achieved. The requirement of high temperatures is a

necessary condition to enhance reaction rates substantially as most solids do not react with each other at room temperature.

These reactions are carried out using different techniques such as ceramic method, carbothermal reduction, combustion synthesis and sintering. The *three* important factors that manipulate *the rate of reaction between solids* are:

1) The area of contact between the reacting solids and their surface area:

It is a crucial factor that the maximum surfaces of all the reactants be in intimate contact for the reaction to occur effectively. Processes such as grinding, milling, spray, drying, etc are exploited to augment the surface area. Pressing the reacting powder into a pellet at relatively high pressure may enhance the contact area of reacting species.

2) The rate of nucleation of the product phase: Rate of nucleation is an important parameter which determines the particles size and size distribution of the final product. Many solid state reactions may involve heterogeneous nucleation governed by topotactic and epitactic reactions. A *topotactic* transformation is characterized by internal atomic displacements, which may include loss or gain of material so that the initial and final lattices are in coherence. *Epitaxy* refers to the growth of the crystals of one mineral on the crystal face of another mineral, such that the crystalline substrates of both minerals have the same structural orientation. The rate of nucleation is dominated by many factors such as the concentration of reacting species, reaction time, temperature, etc.

3) Rates of diffusion of ions through the various phases: Rate of diffusion of ions follows - i) Fick's first law and ii) Tamman's rule.

i) *Fick's first law* relates the diffusive flux to the concentration under the assumption of steady state. It is stated as in equation 2.9.

$$J = -D \left(\frac{dc}{dx} \right) \text{-----[2.9]}$$

where, J = Flux of diffusing species (#/cm²-s)

D = Diffusion coefficient (cm²/s)

(dc/dx) = Concentration Gradient (#/cm⁴)

The average distance a diffusing species will travel, <x>, is given by:

$$\langle x \rangle = (2Dt)^{1/2} \quad \text{where, } t \text{ is the time.}$$

Generally, to obtain good rates of reaction, the diffusion coefficients larger than ~ 10-12 cm²/s are needed. The diffusion coefficient increases with

temperature rapidly as the melting point is approached. This concept leads to *Tamman's Rule*.

ii) *Tamman's rule* suggests a temperature of about two-thirds of the melting point of the lower melting reactant is needed to have reaction to occur in a reasonable time. Based on the above discussion it is clear that the diffusion rate can be increased by:

- **Increase in temperature** induces basically thermodynamical and kinematical conditions which favour diffusion of reacting species.
- **Introduction of defects** by starting with reagents that decompose prior to or during reaction, such as carbonates or nitrates and organometallic compounds.

Steps in Conventional Solid State Synthesis:

Algorithm of the steps involved in a typical solid-state reaction method are represented in figure 2.6.

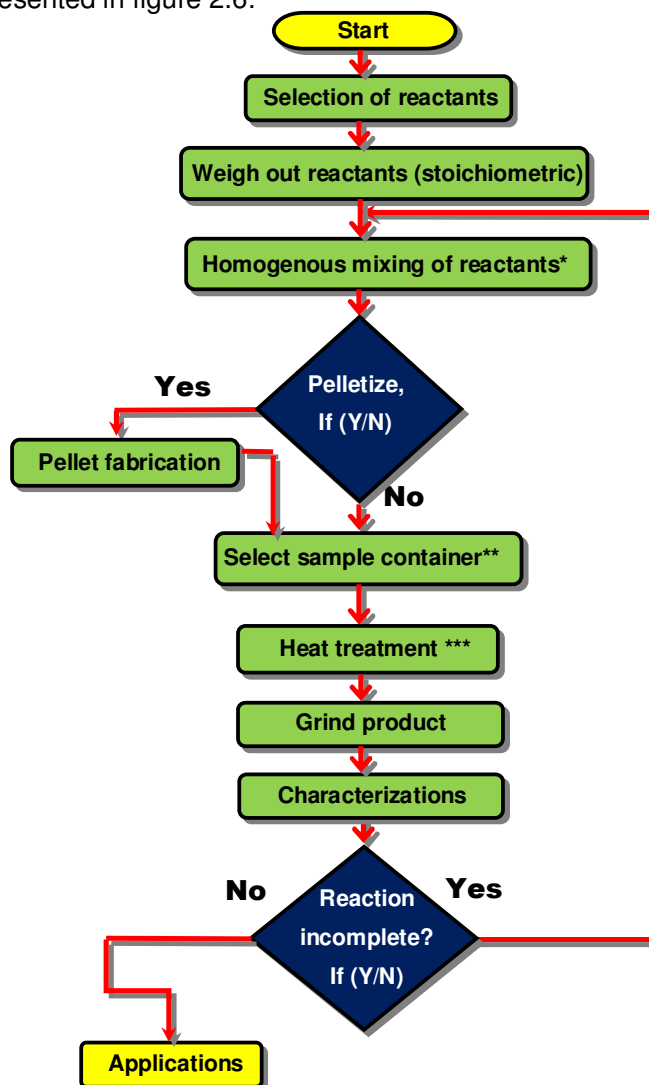


Figure 2.6 Flowchart of conventional solid state synthesis.

Note: 1) *Homogenous mixing of reactants is carried out by using agate mortar & pestle or by ball milling (especially for large preparations > 20 g). Sometimes meagre quantity of volatile organic solvent such as acetone is needed for proper homogenous mixing when agate mortar & pestle is used. 2) ** Selection of sample container depends on the chemical reactivity of reactants, the temperature of reactions and strength, cost & ductility desired from the container. Different types of available containers are: a) Ceramic Refractories (crucibles and boats) e.g. Al_2O_3 , $\text{ZrO}_2/\text{Y}_2\text{O}_3$, b) Precious Metals (crucibles, boats and tubes) e.g. Pt, Au and c) Sealed Tubes e.g. SiO_2 -Quartz, Au, Ag, Pt and 3) ***Judicious choice of heat treatment cycle is a precondition which influences the choice of temperature for volatilization. Additionally, initiation of the heating cycle with lower temperature can help to prevent spillage and volatilization. The atmosphere in which heating is carried out is also a critical parameter. Reactions corresponding to the synthesis of oxides can be either carried out under oxidizing conditions (Air, O_2 , Low temperature) or oxides reducing conditions (H_2/Ar , CO/CO_2 , High temperature). NH_3 or inert (N_2 , Ar, etc.) atmosphere and H_2S atmosphere is maintained for reactions about the synthesis of nitrides and sulfides, respectively. Reaction carried out in sealed tube, or vacuum furnaces may harbor their predetermined atmospheric conditions.

Advantages of solid state reactions:

The benefits of solid state reactions permeate through many industries. It is important economically because the elimination of solvents leads to cost reduction of the products. Some benefits of solid-solid reaction are enlisted as:

- 1) *Eco-friendly 'green' reaction as solvent washing is eliminated.*
- 2) *Unwanted by-products are not generated.*
- 3) *Reduced the number of processing steps.*
- 4) *Thermodynamically stable crystalline products are formed.*

However, this technique also suffers from few disadvantages which are:

- 1) *The reaction time may be longer.*
- 2) *Relatively higher temperature is required.*
- 3) *Occasionally, inhomogeneity in product mixtures is obtained.*

Some of these disadvantages can be overcome by employing certain strategies such as homogenous mixing using a trace amount of volatile solvent, selection of highly reactive precursors, etc.

Application of solid state reaction to nanomaterials synthesis:

Unfortunately, solid state reaction is not very popular in connection with the synthesis of nanomaterials. As mentioned earlier, it is exploited to some extent for the synthesis of ferrites including their nanoparticles. Furthermore, there are few reports on the synthesis of polymer nanocomposites using solid state reaction. A concise outline for synthesis of nanomaterials using solid state reaction is presented in Table 2.3.

Sr. No.	Nanomaterial	Morphology	Reference
1.	ZnO	nanorods	[35]
2.	LiMnPO ₄	nanorods	[36]
3.	PbS	nanoparticles	[37]
4.	SnO ₂ /NiO	nanostucturs	[38]
5.	ZnSnO ₃	nanocubes	[39]
6	TiO ₂	mesostructures	[40]
7	MgFe ₂ O ₄	nanocrystalline	[34]
8	SiO ₂ , CeO ₂ , SnO ₂	nanoparticles	[41]
9	SnO ₂	nanocrystals	[42]
10	NiO	nanoparticles	[43]
11	CdS	nanoparticles	[44]
12	Ag/Ag ₂ S	nanoparticles	[45]
13	CoS	nanoparticles	[46]
14	PbS	nanorods	[47]
15	ZnS	quantum dots	[48]

Table 2.3 Synthesis of nanomaterials using solid state reaction.

As inferred from Table 2.3, solid state reaction is turning out to be promising as far as a synthesis of polymer nanocomposites is concerned [43-47]. To the best of our knowledge, this method is not yet utilized for *in-situ* nanocomposites fabrication belonging to the family of molybdenum compounds viz. Mo, MoO₃, MoS₂, etc. within the polymer matrix. Anticipating the tremendous technological implications in futuristic advanced multifunctional devices, solid state reaction has been probed for the *in-situ*

fabrication of nanocomposites of Mo-MoO₃-PPS and MoO₃-PPS in the present work.

2.2.4 Sol-gel route

Traditionally, sol-gel processing refers to the hydrolysis and condensation of alkoxide-based precursors such as Si(OEt)₄ (tetraethyl orthosilicate, or TEOS). The earliest examples of such reactions date to the work of Ebelmen in 1846. However, at present, sol-gel is not related to alkoxide-based precursors only. Disregarding the nature of the precursors, the sol-gel process can be characterized by a series of distinct steps.

Step 1: Formation of stable solutions of the alkoxide or solvated metal precursor (the sol).

Step 2: Gelation resulting from the formation of an oxide- or alcohol-bridged network (the gel) by a polycondensation or polyesterification reaction that results in a dramatic increase in the viscosity of the solution. If so desired, the gel may be cast into a mold during this step.

Step 3: Aging of the gel (syneresis), during which the polycondensation reactions continue until the gel transforms into a solid mass, accompanied by contraction of the gel network and expulsion of solvent from the gel pores. Ostwald ripening and phase transformations may occur concurrently with syneresis. The aging process of gels can exceed 7 days and is critical to the prevention of cracks in gels that have been cast.

Step 4: Drying of the gel, when water and other volatile liquids are removed from the gel network. This process is complicated due to fundamental changes in the structure of the gel. The drying process has itself been broken into four distinct steps: (i) the constant rate period, (ii) the critical point, (iii) the first falling rate period, and (iv) the second falling rate period. If isolated by thermal evaporation, the resulting monolith is termed as xerogel (figure 2.7). If the solvent is extracted under supercritical or near supercritical conditions, the product is an aerogel (figure 2.7).

Step 5: Dehydration, during which surface-bound M-OH groups are removed, thereby stabilizing the gel against rehydration. This is usually achieved by calcining the monolith at temperatures up to 800 °C.

Step 6: Densification and decomposition of the gels at high temperatures (generally, T > 800 °C). The pores of the gel network are collapsed, and remaining organic species are volatilized. This step is normally reserved for the preparation of dense ceramics or glasses.

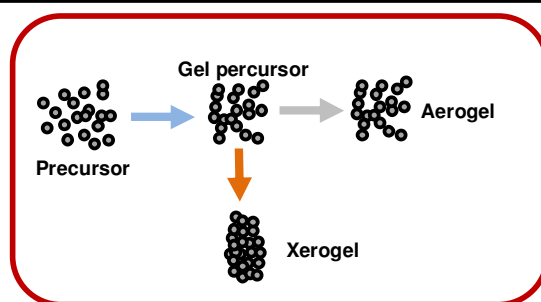


Figure 2.7 Schematic of aerogel and xerogel, two types of sol-gels [49].

This is one of the most preferred chemical techniques for large scale synthesis of nanoparticles, especially oxide nanoparticles. However, it suffers from enormous reaction time scale (in days). Also, in most of the cases, thermal processing (above 800 °C) is required to obtain the final product in crystalline form. So far, the sol-gel method has been extensively used for the synthesis of various nanostructures especially, oxide nanostructures. Few illustrative examples, of synthesized nanostructures using sol-gel route, are given in Table 2.4.

Sr.No	Nanomaterials	Morphology	Reference
1.	$\text{Li}_2\text{MnSiO}_4$	Spherical Nanoparticles	[50]
2.	Fe_3O_4	Uniform shells	[51]
3.	$\text{Fe}_2\text{O}_3, \text{SiO}_2$	Nanoparticles	[52]
4.	Fe_3O_4	Nanoparticles	[53]
5.	ZnO	Nanoparticles	[54]
6.	HfO_2	Spherical	[55]
7.	NiO	Nanoparticles	[56]
8.	CdS	Nanowires	[57]
9.	Au–Pd, Au–Ag, and Au–Pt	Bimetallic nanoparticles	[58]
10.	Fe_2O_3	Nanoparticles	[59]

Table 2.4 Synthesis of nanomaterials using sol-gel route.

The sol-gel method can be modified as per the requirements by combining it with other methods. For example, it can be coupled with microwaves or ultrasonic waves to modify the morphology of final nanoscale products [60]. In the present case, conventional and sonochemical assisted sol-gel methods have been used for the synthesis of MoO_3 nanostructures. In this regard, ultrasonication offers great potential in the processing of liquids and slurries, by

improving the mixing and chemical reactions in various applications and industries. Ultrasonication generates alternating low-pressure and high-pressure waves in liquids, leading to the formation and violent collapse of small vacuum bubbles [61]. This phenomenon is termed cavitations and causes high-speed impinging liquid jets and strong hydrodynamic shear-forces. The extremely high temperatures (>5000 K) and pressure (>20 Mpa) and very high cooling rates ($>10^7$ K s⁻¹) [62] attained during acoustic cavitation lead to many unique properties in the irradiated solution. Furthermore, chemical reactions benefit from the free radicals created by the cavitation as well as from the energy input and the material transfer through boundary layers. For many processes, this sonochemical effect leads to a substantial reduction in the reaction time. Additionally, in chemical kinetics, it has been observed that ultrasound can significantly enhance chemical reactivity in some systems by as much as a millionfold; effectively acting as a catalyst by exciting the atomic and molecular modes of the system (such as the vibrational, rotational, and translational modes). Due to such change in the reaction kinetics, the sonochemical route is capable of producing various types of nanostructures either singly or in combination with other methods such as sol-gel [60, 57, 58, 59]. Sonochemistry can be performed by using a bath (usually used for ultrasonic cleaning) or with a high power probe, called an ultrasonic horn. In our case, the sonochemical assisted sol-gel synthesis of nanomaterials has been carried out using the ultrasonic horn. Schematic showing the synthesis protocol using conventional as well as sonochemical assisted sol-gel route is depicted in figure 5.1 of chapter 5.

In digest, hydro/solvothermal, as well as solid state reaction and sol-gel routes, have their advantages within their limit of synthesis potential. Keeping their benefits and detrimental effects in mind, these three techniques have been strategically employed for the synthesis of Mo, MoO₃, MoS₂ and their combinatorial nanocomposites. At this juncture, it is quite logical to provide a succinct discussion about the materials which have been selected for the present dissertation as elaborately described in the subsequent section 2.3 of this chapter.

2.3. Materials Assortment

Metallic molybdenum (Mo), molybdenum trioxide (MoO₃) and molybdenum disulfide (MoS₂) have been selected as representative materials from molybdenum family. A concise synopsis regarding their synthesis, properties and application potential, is provided through the preceding discussion.

2.3.1 Metallic molybdenum

Molybdenum (Mo) is one of an essential elements in modern technology. It is also a crucial microelement in living organisms, including humans. Molybdenum is an important refractory metal: it has a very high melting point (2623 °C), high electrical conductivity (53.4 nΩ·m (at 20 °C)) and toughness (Young's modulus ~329 GPa, Shear modulus ~126 GPa). It exists in the body-centered cubic crystal structure (BCC) as shown in figure 2.8. It possesses oxidation states: 6, 5, 4, 3, 2, 1, -1, -2 (a strongly acidic oxide). Owing to the abundance of oxidation states, it can form a variety of chalcogenide compounds. From the sulfides so imaginable, only Mo(V), Mo(IV), Mo(III), Mo(VI) and Mo(II) ones have been reported and are discussed with more or less certitude [63]. The examples include MoS₂, MoS₃, Mo₂S₃, Mo₁₅S₁₉, Mo₆S₈, MoS₄, etc. Similarly, from oxides point of view, MoO_x comprises simple binary oxides, namely, MoO₃ and MoO₂, Mo₉O₂₆, etc. MoO₃ has several polymorphs, α-MoO₃, β-MoO₃, ε-MoO₃, and hexagonal (h-MoO₃) [64]. Among these compounds, MoS₂ and MoO₃ (especially, α-MoO₃) are both technologically and fundamentally an important class of materials. Therefore, the synthesis and application aspects of metallic Mo, as well as semiconducting MoS₂ and MoO₃, have been extensively explored in this thesis work.

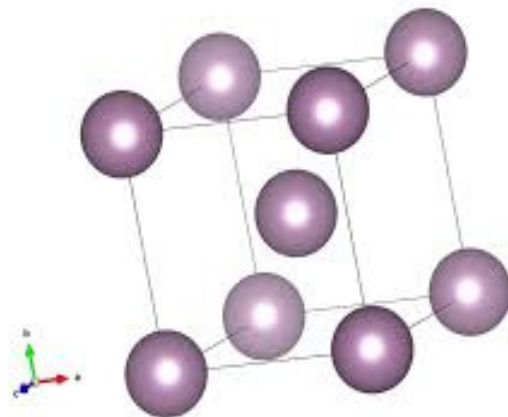


Figure 2.8 BCC crystal structure of metallic molybdenum [65].

Despite being the material with the sixth-highest melting point of any element, molybdenum at present is mostly being used as an alloy material in the steel industry. However, metallic molybdenum is gaining importance in its nano-scale form since molybdenum nanoparticles (Mo-NPs) have a broad range of applications in electronic industry, cutting tools, hard alloys, textiles, microelectronic films, coatings, plastics, and X-ray tubes [66]. Hitherto, there

are very few reports available in the literature on the studies concerning Mo-NPs. Molybdenum nanoclusters have been identified as a prime candidate for electrochemical ammonia production with seemingly low Faradaic losses to hydrogen evolution [67]. Mo nanowires have displayed excellent field emission behavior [68]. A colloidal solution of molybdenum nanoparticles was obtained by Taran et al. via metal dispersion by electric current pulses with an amplitude of 100 to 2,000 A in water [69]. They studied the use of these colloidal Mo solutions as micronutrients to enhance plant resistance to unfavorable environmental conditions and ensure high yields of food crops due to the active penetration of nano-elements into the plant cells. The frictional anisotropy and deformation behavior of a nanostructured thin film consisting of tilted Mo nanorods was investigated by Mohanty et al. [70]. The strength of Mo nanorods was measured under uniaxial tension and was found to be 19.8 GPa, or 7.5% of Young's modulus [71]. For this investigation, the nanorods were prepared by electrochemically etching 99.998% pure molybdenum wires in 1N KOH solution. Mandal et al. reported the synthesis of various types of molybdenum nanoparticles using the in-situ minuscule amount of radioactivity by introducing the radioisotope ^{99}Mo into the solution of ammonium molybdate [72]. Park et al. synthesized molybdenum nanoparticles by RF Plasma [73]. Nanoparticles of Mo were also prepared on the Au substrate by two methods: physical vapor deposition of Mo and UV-assisted chemical vapor deposition through a molybdenum hexacarbonyl precursor for reactivity studies of desulfurization and the formation of MoS_x nanoparticles [74]. Purohit et al. have synthesized nanostructured molybdenum film by electron cyclotron resonance plasma [75]. DC magnetron sputtering [69, 76] has been reported as an important technique for the synthesis of Mo nanostructures. Giovanni et al. have predicted that molybdenum nanoparticles can be used as labels in electrochemical biosensors [77].

In a nutshell, there are sporadic reports pertaining to the synthesis and applications of metallic molybdenum nanostructures even though it is a promising material and should be explored more. Obtaining a metal-metal oxide/sulfide can be substantial from the standpoint of various technological applications. Especially, the interfacial interaction of metal and metal oxide can generate the avenues for their applications as advanced multifunctional devices and components. Precisely documented examples are the incorporation of plasmonic noble metals such as gold and silver nanoparticles along with materials such as TiO_2 , ZnO, etc for catalytic, environmental and

sensor applications [76, 77]. In this context, obtaining Mo-MoO₃/MoS₂ nanostructures can be useful from the standpoint of possible applications in biosensing, catalysis, antimicrobial components, etc.

To the best of our knowledge, there are only three reports corresponding to the synthesis of Mo-MoO₃/ MoS₂ nanostructures as outlined below:

- a) High yields of Mo/MoS₂ inorganic fullerene-like and actinomorphic nanospheres with a core-shell structure have been successfully achieved by the one-step reaction of sulfur and molybdenum nanospheres under a hydrogen atmosphere. This reaction was preceded by preparation of Mo nanospheres by the wire electrical explosion method [78].
- b) Zhou et al. have developed a novel producer for growing well-aligned nanowires arrays of Mo/MoO₃ at nearly 1100 °C [68].
- c) Polycrystalline Mo/MoO₃ nanoflakes have been prepared via thermal decomposition of molybdenum carbonyl in the presence of oleic acid as stabilizing surfactant [79].

However, it may be noted that most of the above-mentioned techniques pertaining to the synthesis of Mo as well as Mo-MoS₂/ MoO₃ nanostructures are energy intensive and required costly vacuum-based equipment for production. Therefore, there is a need to develop a facile and economical technique for the synthesis of such nanostructures in order to realize their hi-tech applications in various fields. Driven by this desire, facile solid-solid reaction route (briefly described in Section 2.2.3 of the present chapter) has been explored for the concurrent and in-situ generation of Mo-MoO₃ nanostructures entrapped in the polymer matrix.

2.3.2 Molybdenum oxide

The field of transition metal oxides represents an exciting and rapidly expanding research area that spans the border between the physical and engineering sciences. Molybdenum oxides (MoO_x) are one of the most attractive metal oxides due to their special structural characteristics. MoO_x comprises simple binary oxides, namely, MoO₃, MoO₂, and Mo₉O₂₆.

MoO₃ has several polymorphs, such as the thermodynamically stable α -MoO₃ (space group *Pbnm*), metastable β -MoO₃ (*P2₁/c*), ϵ -MoO₃ (*P2₁/m*), and hexagonal metastable h-MoO₃ (*P6₃/m*) [80]. MoO₂, with its distorted rutile structure, is an unusual but interesting transition metal oxide because of its low metallic electrical resistivity ($8.8 \times 10^{-5} \Omega \cdot \text{cm}$ at 300 K in bulk samples), high melting point, and high chemical stability [81]. MoO₂ has been used as a catalyst for alkane isomerization [82], oxidation reaction [83] and as a gas

sensor [84]. It is also a promising anode material for Li-ion batteries [85]. The hexagonal phase of MoO_3 is also very interesting metastable phase due to its one dimensional (1D) behaviour and the tunnel structure, which exhibits superior photo-physical and photo-chemical properties [86]. $h\text{-MoO}_3$ NCs acts as an appropriate visible light driven photocatalyst as the optical band gap lies in the visible light region (2.8–3.0 eV), which can directly absorb visible light photons [86].

Molybdenite or $\alpha\text{-MoO}_3$ (stable phase) is the most important among all the polymorphs of MoO_3 . $\alpha\text{-MoO}_3$ consists of corner-sharing chains of a double layer of zigzag MoO_6 octahedra held together by covalent forces in the a - and c - axis directions and by weak van der Waals forces in the b -axis direction and exhibits an intrinsic variability in its oxygen content [87]. The oxidation state of molybdenum in this compound is +6. The crystal structure of $\alpha\text{-MoO}_3$ is depicted in figure 2.9. $\alpha\text{-MoO}_3$ is a wide band gap (3.2 eV) n -type semiconductor and a well-known electrochromic, photochromic, and display material (Zhou et al. 2003) [88]. MoO_3 was used as a catalyst for oxidation of hydrocarbon, alcohol, propane, methane and reduction of NO_x [89]. Recently, MoO_3 has been attracted as a new gas sensing material and found to be responding to both oxidizing (NO_x) and reducing gases (H_2 , NH_3 , and CO ; Barazzouk et al. 2006 [90]; Sunu et al. 2003 [91]; Imawan et al. 2001 [92]. MoO_3 is one of the most interesting materials, because of its nontoxic nature and the very deep lying electronic states and therefore, nano-suspension of MoO_3 has been incorporated as hole extraction layer in polymer solar cells and demonstrated the replacement of the commonly employed semiconductor polymers [93, 94]. In the field of energy storage domain, it is being explored as a cathode material in the Li-ion batteries as well as pseudocapacitor material please refer to Table 2.5 refer for the pertinent information.

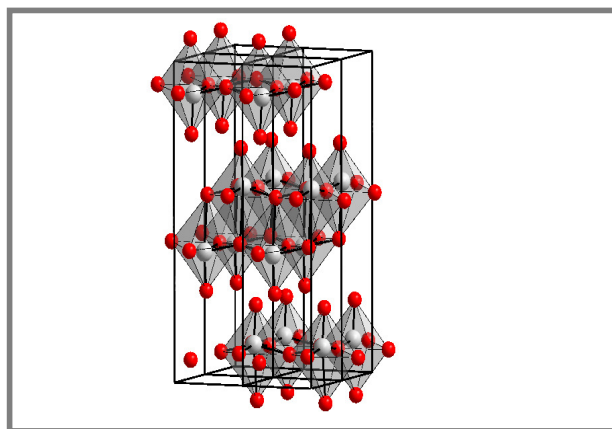


Figure 2.9 Crystal structure of $\alpha\text{-MoO}_3$ [95].

Summary of the recent progress towards the synthesis and applications of MoO₃ nanostructures is presented in Table 2.5. It can be concluded that still there is a need to design a methodology of facile, economical and environmentally friendly process for the synthesis of molybdenum oxide nanostructures with tuned morphologies preferably entrapped within the polymer matrix to realize their nano-material based device fabrication potential. For this purpose, we have explored solid-solid reaction route for the fabrication of MoO₃-polymer NCs. For the synthesis of plain MoO₃ nanostructures, hitherto unreported conventional and ultrasonication assisted sol-gel method has been employed which is easy and is capable of gram scale production of nanostructures. The description related to solid-solid reaction route has been presented in section 2.2.3.

Sr. No.	Synthesis method	Phase/Morphology	Application (if any)	Reference
1	Hydrothermal	α -MoO ₃ nanobelts	Cathode material of a Li-ion battery	[96]
2	Chemical precipitation	h-MoO ₃ nanocrystals	Cathode Photocatalytic degradation of methylene blue	[97]
3	Solvothermal	α -MoO ₃ nanoparticles	H ₂ S gas sensing	[89]
4	Hydrothermal	Single-crystal nanostructures of α -MoO ₃	----	[98]
5	Hydrothermal	α -MoO ₃ nanorods	Lithium storage properties	[99]
6	Co-precipitation	Mesoporous crystalline MoO ₃	Pseudocapacitor	[100]
7	Hydrothermal (140–200 °C)	α -MoO ₃ nanorods	----	[101]
8	Atmospheric,	Flower-like α -	----	[102]

	flame synthesis	MoO ₃ nanobelt arrays		
9	Hydrothermal	Ultralong α-MoO ₃ nanobelts	Lithium storage	[103]
10	Solvothermal	Flower-like α- MoO ₃ with hierarchical structure	Triethylamine sensor	[104]
11	Hydrothermal	Flexible Single crystalline MoO ₃ nanobelts	Cathode material for rechargeable Li-ion batteries	[105]
12	Hydrothermal	h-MoO ₃ nanobelts	Cathode Photochromic and electrochromic	[106]
13	Chemical precipitation	Helical nanosheets, crosslike nanoflowers, and nanobelts	----	[107]
14	Hydrothermal	Single crystalline MoO ₃ nanofibers	Cathode material of a Li-ion battery	[108]
15	Electrodeposition	α- and β-phase MoO ₃	Gasochromic	[109]
16	Hydrothermal	α-MoO ₃ nanobelts	Li-ion batteries	[110]
17	Evaporation assist deposition	Single crystalline MoO ₃ nanobelts	-----	[111]
18	<i>Ex-situ</i> intercalation	Highly b-axis oriented MoO ₃ film	Volatile organic compound gas- sensing	[112]

19	Hydrothermal	α -MoO ₃ nanoribbon	Hydro- desulfurization catalyst	[113]
20	RF magnetron sputtering	MoO ₃ Nanorods, bundled nanowires and nanoslabs	Gas sensing	[114]
21	Thermal evaporation in air	Crystalline microbelt MoO ₃	Field emission	[115]
22	Electro-spinning	Single- crystals MoO ₃ nanowires	Biochemistry sensing probes	[116]

Table 2.5 Summary of the recent progress towards the synthesis and applications of MoO₃ nanostructures.

2.3.3 Molybdenum sulfide

By far the most studied among the molybdenum sulfides is MoS₂, which finds practical applications in diverse areas. MoS₂ compound is thermodynamically stable with a standard enthalpy of formation of MoS₂ determined by fluorine bomb technique at 298.15 K is $-(65.8 \pm 1.2)$ kcal mol⁻¹ [117]. MoS₂ has a structure built of close-packed layers of sulfur atoms stacked to create trigonal prismatic interstices occupied by molybdenum as shown in figure 2.10. Only relatively weak van der Waals bonding exists between layers, which render lubricant properties to MoS₂ similar to graphite. Crystalline varieties 2H, 3R, and 1T of MoS₂ were reported [118-120]. According to K.T. Park et al. no surface reconstruction or relaxation occurs in the MoS₂ crystal [121]. As follows from the structure, MoS₂ is a highly anisotropic layered material. Thus, electric conductivity parallel to the layer is 1000 times greater than in the perpendicular direction [122].

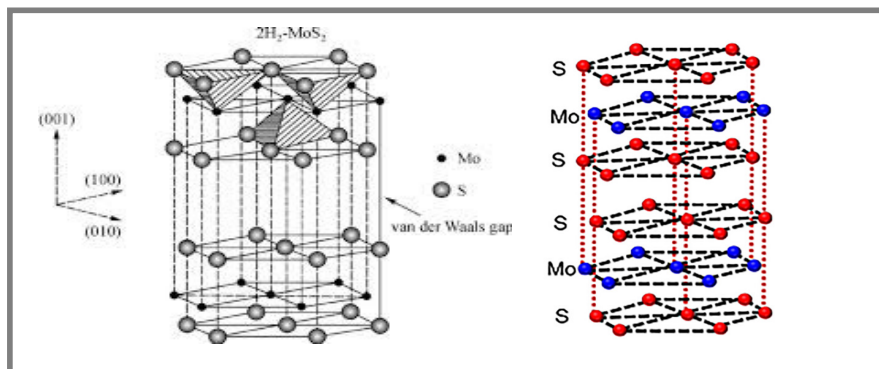


Figure 2.10 Hexagonal crystal structure of MoS_2 [95].

Because of such typical crystal structure of sandwich interlayer of S-Mo-S, MoS_2 is the most famous example from the layered transition metal dichalcogenide family of materials. Bulk MoS_2 is a well known solid lubricant and is also used as hydrodesulfurization catalyst [124] in the petroleum industry. However, at nanoscale MoS_2 transforms into a wonder material which can be attributed to changes in its optical and electronic properties [125,126]. Bulk MoS_2 is semiconducting with an indirect band gap of 1.2 eV [127]. Nevertheless, at nanoscale an increase in band gap is observed and it is found to be transforming into direct band gap semiconductor with a band gap of 1.8 eV for a mono-layered structure [128]. MoS_2 nanotubes and nanowires tend to flaunt the influence of quantum mechanical confinement in their electronic and optical properties [129,130]. Other features that make MoS_2 interesting for applications in areas like nanoelectronics include the absence of dangling bonds and thermal stability up to 1100 °C. Owing to the above attributes, MoS_2 has gained importance as a semiconducting analog of graphene and is predicated as a powerful competitor to silicon in electronic devices. Encouraged by the interesting properties exhibited by MoS_2 at the nanoscale, a broad range of synthesis techniques have been evolved and its is explored for a diverse set of applications in arena ranging from energy generation & storage, optoelectronics, biosensors, etc. A tabular abridgment of different synthesis methods and applications of nanoscale MoS_2 is presented in Table 2.6.

Some methods considered in this condensed review include molecular precursor decomposition, hydrothermal, soft chemistry, aqueous surfactant-aided, ultrasonically assisted, intercalation exfoliation and solid gas reactions.

Sr. No	Synthesis method	Phase/ Morphology	Application (if any)	Referenc e
1	Hydrothermal	Single-molecular-layer	-----	[131]
2	<i>In-situ</i> photo-reduction deposition	Nanoclusters	Photo-catalytic	[132]
3	Direct sulfidization	Submicrometer sheres	-----	[133]
4	Two-step simple hydrothermal	Layered hybrid	Photocatalytic H ₂ production activity.	[134]
5	Chemical vapour deposition	Monolayer	Electronic transport	[135]
6	Two-step thermal reduction of MoO ₃ at 500 °C in H ₂ followed by sulfrization at 1000 °C in the presence of sulfur	Thin layers (Wafer-scale)	FET devices i.e electronics and optoelectronics.	[136]
7	Chemical vapour deposition	Hybrid heterostuctures	-----	[137]
8	Chemical vapour deposition	Hollow fullerene-like	-----	[138]
9	Chemical vapour deposition	Highly flexible thin-film	Transistors and flexible electronics	[139]
10	Mechanical cleavage and scotch-tape exfoliation techniques	Monolayer, sub-nanometer.	Transistors	[140]
11	Electro-chemical	Micrometer-sized,	Anode	[141]

		small plate like and layered	material for lithium ion batteries	
12	Catalyzed transport reaction including C₆₀ as a growth promoter	Self-assembly of single-wall sub-nanometer-diameter molybdenum disulfide tubes	-----	[142]
13	Micro-exfoliation	Electronic structure of bulk and monolayer MoS ₂	-----	[143]
14	Co-assembly of organic and inorganic precursors	Lamellar nanocomposites	Opto-electronic	[144]
15	Two-step thermal reduction of MoO₃ in H₂ followed by sulfuration in the presence of H₂S.	Closed cage structure (fullerene-like) of nanoparticles	Nano-particles for solid lubrication	[145]
16	High-temperature sulfidation of Mo initially deposited onto a clean Au(111) single-crystal	Atomic-scale structure of nanoclusters	Hydro-desulfurization catalysts	[146]
17	Chemical bath deposition	Poorly crystalline thin film	-----	[147]
18	High-temperature sulfidation of Mo initially deposited onto a clean Au(111)	Nanoparticulate	Hydrogen evolution reaction catalysis	[148]

	single-crystal			
19	Hydrothermal	Amorphous nanofiber bundles	----	[149]
20	Micelle-assisted route	Inorganic fullerene-like nanospheres	-----	[150]
21	Precipitation in turbulent micromixers	Nanoparticles	Lubricant	[151]
22	Micromachining	Nanobelts	----	[152]
23	Ultrasonic spray pyrolysis	Porous	Hydrodesulfurization catalyst	[153]
24	Mechanochemical solid-state reaction	Laminar structures	-----	[154]
25	Mechanical activation	Nanoflakes	----	[155]
26	Room temperature sonoelectrochemical	Fullerene-like nanoparticles	----	[156]
27	Sonochemical	Nanoparticles	----	[157]
28	Gas–solid reaction	Open-ended nanotubes	Catalyst for methanation of carbon monoxide with hydrogen	[158]
29	Hydrothermal treatment	Nanotubes and nanocoils	-----	[159]

Table 2.6 Condensed review of synthesis and applications of MoS₂ nanostructures.

2.3.4 Poly(phenylene sulfide)

Poly(phenylene sulfide) or PPS is a crucial polymeric material constituting a series of alternating aromatic rings and sulfur atoms (Figure 2.11.) and is precisely referred as Poly(p-phenylene sulfide). PPS is a high-quality engineering polymer. Charles Friedel and James Mason Crafts discovered

PPS way back in 1888 [160]. Edmonds and Hill of Phillips Petroleum Company modified the method of PPS production using p-dichlorobenzene and sodium sulfide in 1967 [161]. Subsequently, the commercial production of PPS started in 1972.

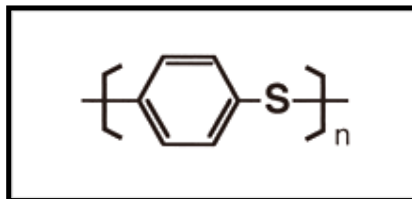


Figure 2.11 Basic building block of PPS [162].

Properties

PPS is a semi-crystalline material exhibiting an excellent blend of properties, namely, high-temperature resistance, chemical resistance, flow ability, dimensional stability, and electrical characteristics. Being a brittle material, PPS must be incorporated with fibers and fillers to realize improvement in its properties and applications. The properties of PPS are categorized below:

- ❖ *Mechanical Properties:* PPS is brittle and notch sensitive. Because of its low melt viscosity, PPS can be molded with high loadings of fillers or reinforcing materials. The fillers and reinforcing materials enhance the strength, dimensional stability, and other properties.
- ❖ *Thermal Properties:* PPS exhibits flame retardancy and thus is ideal for high-temperature electrical applications. Comparatively, PPS demonstrate high thermal stability as evinced from its differential scanning calorimetry (DSC) and thermogravimetric analysis (TGA) results. PPS illustrates a glass transition temperature (T_g) of 85–90° C, melting temperature ~ 285° C, the onset of thermal degradation at 430° C and pyrolysis temperatures up to 550° C [163].
- ❖ *Optical Properties:* Unstabilized PPS tends to degrade in sunlight caused by the overlap of the absorption spectrum of PPS with the ultraviolet region of the solar spectrum. A systematic study [164,165] conducted to find suitable light stabilizers (such as UV absorbers, quenchers, and antioxidants) has revealed that successful photostabilization of PPS can be achieved by using UV absorbers rather than quencher-type additives.
- ❖ *Solubility:* The polymer has a broad compatibility with chemicals and solvents, offering a better chemical resistance than stainless steel. No solvent for PPS is known below 200°C. Above this temperature, 1-

chloronaphthalene is a suitable solvent. However, this attribute of the low solubility of PPS in most of the solvents hinders its processability and in turn, its usability.

- ❖ *Electrical Properties:* PPS is an excellent electrical insulator, even at high temperatures. The volume resistivity and the dielectric strength remain high up to 200° C. The polymers have a low dielectric constant and a low loss factor throughout a wide temperature range. Nevertheless, the PPS dielectric constant of 3.0 is equivalent to that of polyester and polycarbonate, and 35% greater than polypropylene.

Owing to these properties PPS has potential for relatively high-temperature dielectric capacitor applications apart from its routine insulator material based applications. The capacitor applications may include: a) High temperature high-frequency AC at 125° C internal temperatures, b) Surface mount devices for wave or vapor phase soldering at 240° C and c) Intermittent high temperature, reliable operation at 125° C ambient. Hitherto, PPS has not been explored as a suitable choice of polymeric host for the development of polymer nanocomposites due to its limitation of solubility in a variety of solvents. Ingenious choice of solid state reaction may help to overcome this limitation. Inspired by this hypothesis, *in-situ* synthesis of Mo-MoO₃-PPS and MoO₃-PPS has been conducted as a part of this dissertation.

2.4. Characterization Tools for Nanomaterials

Advanced nanotechnology engaged numerous key steps. First is the size and shape controlled the synthesis of nanomaterials and second involves synthesis and characterization nanoparticles for developing the nanodevices and nanostructures to understand the behavior and properties of nanoparticles, ultimately aiming at implementing nanotechnology, controlling their behavior and designing new nanomaterials control systems with excellent performance. Third, theoretical modeling is virtually necessary to understand and predict material's performance. Finally, the ultimate goal is to develop an application based on nanomaterials. In consideration of the large diversity of research in nanomaterials, this section of the present chapter 1 concentrates on characterization techniques which are extensively used for studying various properties of nanomaterials. Most of these techniques are employed for characterization of nanostructures synthesized during the course of work of the present thesis. Nanomaterials characterization can be carried out using (a) *Microscopy techniques:* These techniques provide the information about appearance, morphology (size and shape) and presence of defects (in case of high resolution techniques), and (b)

Structural and Spectroscopy techniques: These techniques provide information like structure, phase, bonding state, band gap (in case of semiconductors), electronic transitions, doping, and defects, etc. However, it may be noted that both techniques are required for better understanding of the physicochemical properties of the materials. Hence, many of the characterization instruments incorporate both microscopy as well as spectroscopy aspects into their instruments. For example, Field emission scanning electron microscopes (FE-SEM) have 'in built' energy dispersive spectroscopes (EDS) as an indispensable part of the instrument. In this section, initially, microscopic techniques used in the present work for characterization of resultant nanostructures will be discussed which will be followed by the spectroscopic and structural identification techniques. In the beginning electron microscopy techniques have been discussed as they have been extensively used. In the end of this section, a brief description of atomic force microscopy (AFM) and confocal laser scanning microscopy (CLSM) is also given.

2.4.1 Microscopy techniques

The ultimate goal of electron microscopy is to determine the structure of materials quantitatively. All the electron microscopies and spectroscopies are based on the interaction of electromagnetic radiation with matter in different regimes [166]. Figure 2.12 depicts the situation in a clear perspective. When a beam of electrons is incident on a specimen to be evaluated, it interacts with the specimen and following major processes take place.

1. Electrons reflected from the surface give rise to secondary electrons (SE) (which penetrate to only 2-3 nm inside specimen) as well as backscattered electrons (BSE) that penetrate few ten nm distance and then are reflected back. These SE and BSE are used for imaging in Scanning Electron Microscopy (SEM) mode.
2. Continuous as well as characteristic X-rays are generated. These characteristic X-rays are atom specific and can be used for obtaining the elemental information of the specimen via Energy Dispersive Spectroscopy (EDS) if equipped along with SEM or TEM.
3. If the specimen is thin enough, then the electrons are transmitted along with them getting elastically and inelastically scattered during the process. These transmitted as well as scattered electrons can also be used for imaging the specimen in Transmission Electron Microscopy (TEM) mode.
4. Heat is also produced in the specimen.

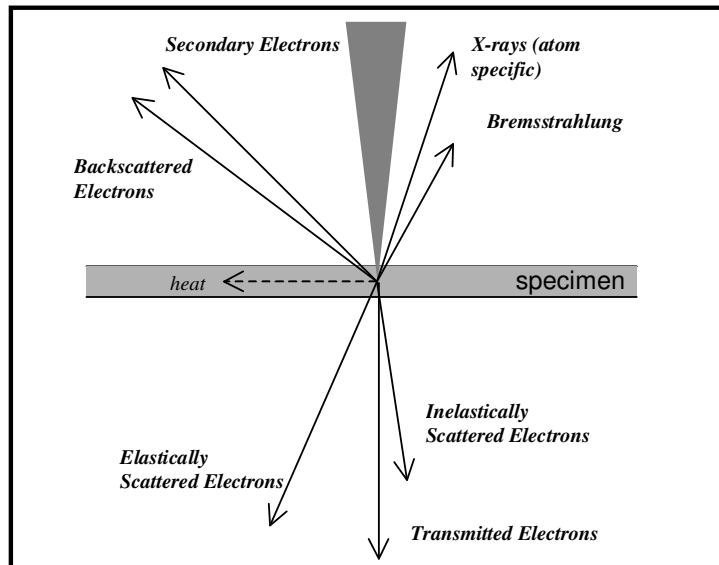


Figure 2.12 Electron beam specimen interaction.

The detailed discussion about imaging using these two main electron microscopy techniques is presented below. Figure 2.13 shows the comparison of an optical microscope (LM), SEM and TEM as far as instrumentation part is concerned.

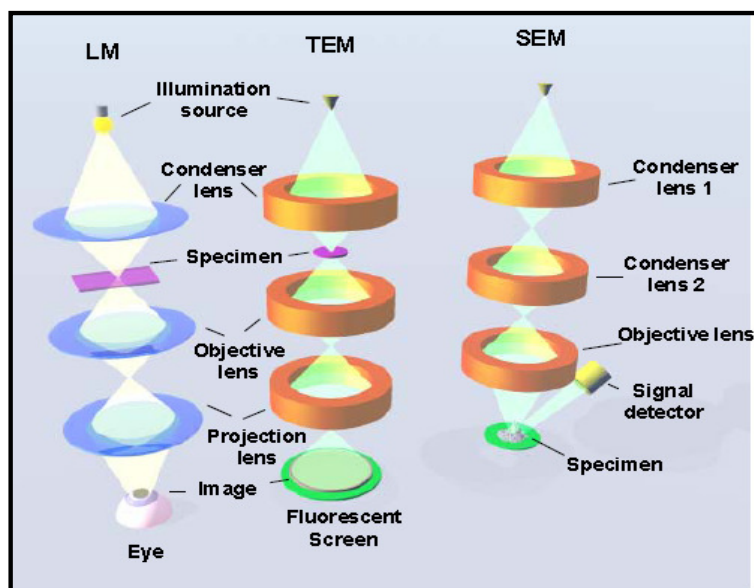


Figure 2.13 Comparison of the LM, TEM, and SEM [166].

2.4.1.1 Scanning electron microscopy

All scanning electron microscopes or SEMs use the scanning principle for imaging (hence the name SEM). The focused electron beam is scanned over the surface of the bulk sample synchronized with the scanning of another electron beam in a TV tube. Any selected signal from the sample (varying as a function of beam position) can modulate the intensity of the TV tube. Magnification is determined by the ratio of the lengths of the two respective scanned lines.

Typical accelerating voltage varies from 30 keV down to 200 eV. Resolution is the best at the higher voltages (~0.2 nm for FEG at 30 keV). The main advantages of SEM is good spatial resolution (intermediate between optical microscopy and TEM), large depth of focus (giving a clear image simultaneously from hills and valleys of a rough surface) and moderate sample preparation. If an X-ray detector is attached (either energy dispersive spectrometer (EDS) or wavelength dispersive spectrometer (WDS)), the analytical capacity becomes close to a microprobe. Working distance is variable in many SEMs; low for high-resolution imaging and large for EDS/WDS. In conventional SEM instruments, thermionic emission (in tungsten cathode) is used to generate the electron beam. This puts a limitation on the resolution of the materials and the magnifications which can be achieved. Hence conventional SEM is not suitable for characterizing the nanometer scale materials. This difficulty is overcome in modern SEM instruments using field emission (FE) gun to achieve the high magnification and better resolution. These instruments are called as Field Emission SEMs or FE-SEMs to differentiate them from the conventional SEMs. For the present work, we have mostly used FE-SEMs owing to the higher magnification and better resolution which is required to image nanoscale materials.

2.4.1.2 Transmission electron microscopy

The first image with a Transmission electron microscopy or TEM was obtained by Ernst Ruska and Max Knoll in 1932. Transmission electron microscopy examines structure by passing electrons through the specimen. The image is formed as a shadow of the specimen on a phosphorescent screen [167]. In order for electrons to pass through the specimen, it must be very thin (usually less than 100 nanometers or approx. 1/25,000 inch) thick. A schematic of a typical TEM is shown in figure 2.13.

The modern electron microscopes are constructed with acceleration voltages as high as 200 kV, 300 kV, 400 kV and even 1250 kV ('atomic resolution' microscope). Elastic scattering is used in the formation of the true electron-optical images by electrons transmitted through the sample. Diffraction contrast dominates low and medium magnification images. High-resolution images are based on phase contrast. Assessment of crystal defects is the main application of conventional TEM. The sample is illuminated by a broad (nearly) parallel beam and the image is formed by the imaging lenses at the other side of the sample. Magnification has nothing to do with the size of the illuminated area; it is determined by the imaging lenses. The image is formed on an electroluminescent screen (or film or detector) in a fixed position in both modes of operation. The possibility to form an intense, fine beam and the presence of an energy dispersive spectroscopy (EDS) or an electron energy loss spectroscopy (EELS) detector makes an are the important aspects of modern TEMs.

A transmission electron microscope uses a series of electromagnetic lenses to manipulate the electron beam generated at a very high potential in an electrically heated filament. Depending on the imaging conditions, whether particle or wave properties of the emitted electrons have to be considered. The wavelength of the electrons depends on the accelerating voltage ($= h/(2meV)^{1/2}$). As an electron wave penetrates the sample, the resulting diffraction pattern reveals the structure of the observed sample. Analyzing the image and corresponding diffraction pattern, one can obtain useful information on grain sizes, the precipitates, and the orientation of the precipitates to the matrix and appearance of the superstructure. With the aid of the energy dispersive X-ray attachment (analytical microscope), it is possible to measure qualitatively and quantitatively the concentration and composition of elements, using the characteristic X-ray spectra. In the transmission electron microscope, one can simultaneously obtain the image and the corresponding diffraction pattern from the same part of the sample and concentration of elements in the sample as well as the mapping of the elements in the same region of the sample. The mapping of the elements is also possible with the scanning probe resolution of 1 nm. Based on the particular diffraction pattern, it is possible to obtain the bright field (BF) as well as the dark field (DF) image. High resolution TEM (HRTEM) provides direct evidence in the local structure and its irregularities at the atomic scale.

SAED and microdiffraction patterns of a crystal permit to obtain the symmetry of its lattice and calculate its inter-planar distances (with the Bragg law). This is useful to confirm the identification of a phase after assumptions generally based on the literature of the studied system and chemical analyses. Conventional TEM uses only the transmitted beams *or* some of the forward scattered beams to create a diffraction contrast image. HRTEM uses the transmitted *and* the scattered beams to create an interference image. Actually, electron crystallography is a complementary technique of X-ray crystallography: the strong interaction between electron and matter (thousands of times stronger than X-rays) enables the structural determination of crystals of a few nanometers size with, in some cases, precisions on the atomic positions comparable to those obtained with X-rays ($\sim 0.02 \text{ \AA}$). As nanotechnology strives to miniaturize components down to the level of interactions between single and multiple atoms, FE-TEM has become the versatile eyes into the nanoworld. Since the FE-TEM generates a fine particle beam as the electron source is a field emitter gun (FEG), the nanochemistry of a superthin material may be analyzed by energy lost as the electron beam passes through a sample, or through X-rays produced by electron substitutions. FEG is far superior electron source as compared to the other the other two i.e. tungsten and lanthanum hexaboride (LaB_6) based ones. The nature of bonds between atoms may be sensitively probed using a planned electron energy loss spectroscopy (EELS) system. Such state of the art FE-TEMs are capable of measuring crystalline properties down to the atomic scale and resolve chemical properties down to the nanoscale.

2.4.1.3 Atomic force microscopy

The first Atomic Force Microscope (AFM) was introduced by G. Binnig and C. Gerber in 1985 [168]. When two atoms are close to each other, there are attractive and repulsive forces which depend upon the distance of their separation. Combined force is given by the equation

$$F = \frac{A}{R^{12}} - \frac{B}{R^6} \text{ -----[2.10]}$$

where F is a resultant force between two atoms, A and B – constants and R is the distance between two atoms. The first term is the repulsive force and the second term is an attractive force between two atoms. It can be seen that repulsive force is more efficient at a very short distance and

changes rapidly with distance. This is due to the repulsive interaction between the electron clouds at a short distance (Pauli exclusion principle). AFM has a flexible cantilever $\sim 100 \mu\text{m}$ long, $10 \mu\text{m}$ wide and $1 \mu\text{m}$ in height attached to a piezo drive. A tip is mounted on cantilever as shown in figure. 2.14 which can be brought close to the sample surface. For cantilever

$$F = K \times \delta z \quad \text{-----}[2.11]$$

where F is force experienced by the cantilever, K is related to the natural resonance frequency of the cantilever (spring constant) and δz is the displacement of the cantilever. Resonant frequency of cantilever is given as

$$(\omega_r) = \sqrt{\frac{\left(K - \frac{\delta F}{\delta z}\right)}{m}} \quad \text{-----} [2.12]$$

The resonant frequency is used to control the tip-sample interaction. AFM tip, in close vicinity of the sample surface, experiences a repulsive force which results into minute amount of bending of the cantilever. A laser beam is directed on back of the cantilever (see figure. 2.14).

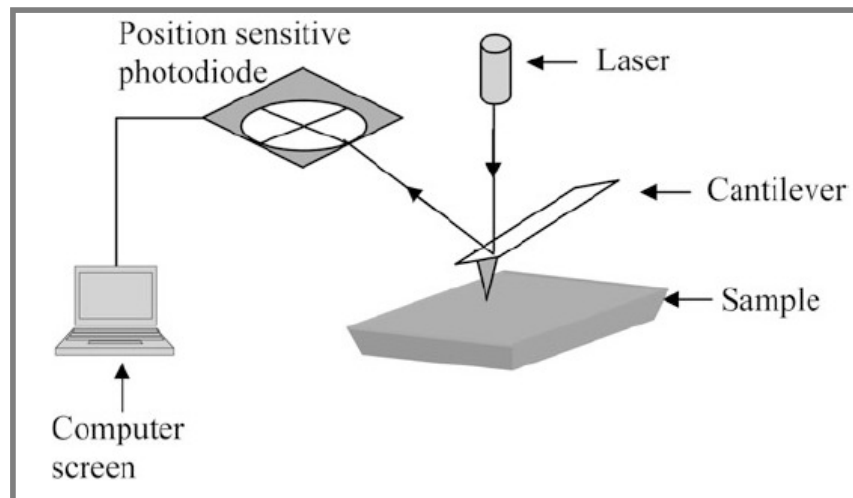


Figure 2.14 Schematic of an Atomic Force Microscope [168].

Small deflections caused by the tip-sample interaction are recorded by a position sensitive photodiode. By rastering, the probe on the sample surface and measuring the cantilever deflections, surface image is obtained. An AFM can be operated in three different modes viz. (1) Contact mode, (2) Noncontact mode and (3) Tapping mode.

Contact mode: In this case, the tip is in contact with the sample surface and is almost forced into it. However, due to a repulsive interaction between electron charge cloud of the tip atom and that of the surface atom, the tip is repelled back which bends the cantilever and deviates the direction of the laser beam. In this mode the interaction due to the first term on right-hand side of equation (2.10) is dominant due to the very small value of ' R ', the distance between two atoms. The main disadvantage of this mode is that the tip or sample can get damaged due to the forcing of the tip into the sample, especially, polymers or other organic materials like biological samples which can get damaged by this method.

Non-contact mode: In non-contact mode, the tip or the probe moves at some small distance away from the sample surface. Therefore, it cannot damage the sample. In this mode the second term on the right-hand side of the Eq. (2.10) is the dominant term. This term arises due to the polarization of interacting atoms and is due to the dipole-dipole interaction of two atoms.

Tapping mode: Tapping mode is a combination of contact and non-contact modes. The resolution in contact mode is higher than that due to non-contact mode because in contact mode the interaction between tip and surface atoms is much more sensitive to the distance as compared to that in non-contact mode. With tapping mode, high resolution advantage of contact mode and non-destructiveness of noncontact mode are achieved. The tip oscillates in the vicinity of the surface at a distance of ~ 50 nm in such a way that it nearly touches the sample during its cycle of oscillation. Tapping mode is simple and robust to use.

2.4.1.4 Confocal microscopy

Resolution of an optical microscope can be improved by limiting the field of view. This is the principle used in a confocal microscope. A confocal microscope can be of transmission or reflection type. In figure 2.15, a ray diagram of a confocal microscope in the transmission mode is illustrated. A point source of light and a small area detector are used in this microscope, which restricts the field of view. The light from the point source is focused on the specimen to cover only a point (or very small area) on the sample. The objective lens, in turn, forms a small image of this illuminated portion on the point detector. It is possible to raster (move in x-y directions or in a plane) the sample so that light falls on each part of the sample and the signal gathered by the detector is used to construct the image.

Alternatively, the point source and detector are synchronously rastered to view the entire specimen and construct the corresponding image. Use of point source and detector improves the depth resolution of a confocal microscope. It is capable of optically sectioning a three-dimensional thick object to a resolution determined by the detected sample volume. The detector uses an aperture which eliminates the light not coming from the focus on the sample and scans the sample in one plane point by point. Image of one plane is stored in a computer.

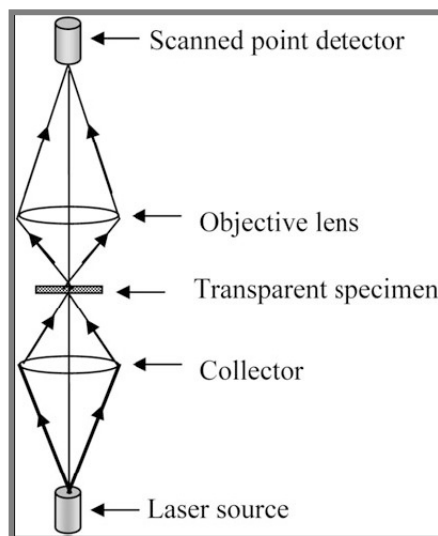


Figure 2.15 Schematic diagram of a confocal microscope in transmission mode [168].

By adjusting the focus of light in a different plane, point by point the entire plane is scanned and image of that plane is stored. The sample is scanned in this fashion to achieve a high resolution 3-D image of the sample. The confocal microscope is therefore widely used in biology to study objects like cells. Either specimen or beam falling on the specimen are synchronously rastered, and image is reconstructed on the computer

2.4.2 Spectroscopy techniques

Before starting with discussion on this technique, it is appropriate to discuss some important aspects about various spectroscopy techniques and the properties they probe. Table 2.7 summarizes all the important spectroscopic tools with respect to the chemistry they probe and their common applications.

Spectroscopic Technique	Region of operation	Probe	Common Features
UV-vis	UV-vis region	Bonding electrons	Quantitative analysis/Beer's Law

Atomic Absorption	UV-vis region	Atomic transitions (valance electron)	Quantitative analysis/Beer's Law
Raman	IR/UV	Vibrations	Functional Group Analysis/quantitative
X-Ray Spectroscopy	X-rays	Inner electrons, elemental	Elemental Analysis
X-ray Crystallography	X-rays	3D structure	3-D structure Analysis
Dynamic limit scatter	Visible	Hydrodynamic particle size	-

Table 2.7 Important spectroscopy techniques and property they probe.

2.4.2.1 X-ray diffraction

X-ray diffraction (XRD) is a material characterization technique that can be useful for analyzing the lattice structure of material. The basic principle behind XRD is Bragg's law of diffraction. Diffraction is a scattering phenomenon [169]. When X-rays are incident on crystalline solids, they are scattered in all directions. In some of these directions, the scattered beams are completely in phase and reinforce one another to form the diffracted beams. The Bragg law describes the conditions under which this would occur (figure 2.16). It is assumed that a perfectly parallel and monochromatic X-ray beam, of wavelength λ , is incident on a crystalline sample at an angle θ .

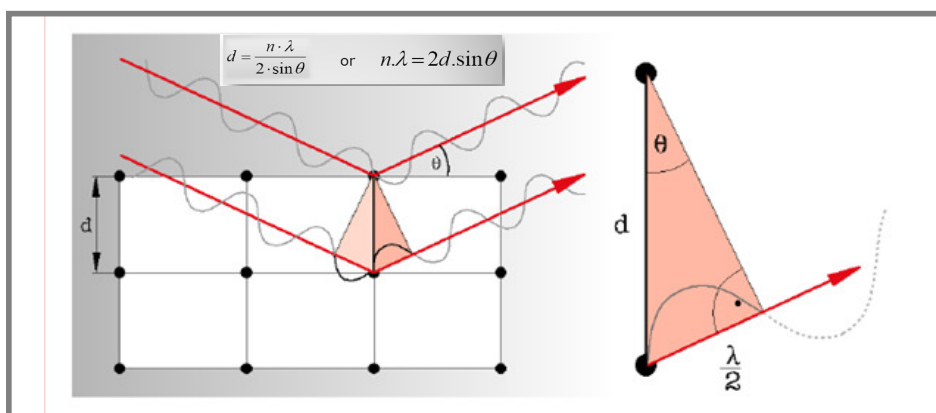


Figure 2.16 Pictorial representation of X-ray diffraction phenomena [169]

According to the Bragg's law diffraction will occur if the following condition is satisfied (figure 2.16):

$$2 d \sin \theta = n \lambda \quad \text{-----}[2.13]$$

Where d is the distance between atomic planes, n an integer (1, 2, ..., n), λ the wavelength, and θ the angle of incidence of the X-ray beam and the atomic planes. $2d \sin\theta$ is the path length difference between two incident X-ray beams where one X-ray beam takes a longer, but parallel, path because it "reflects" off an adjacent atomic plane. This path length difference must equal an integer value of the λ of the incident X-ray beams for constructive interference to occur in such a way that a reinforced diffracted beam is produced. By varying the angle θ , the Bragg's Law conditions are satisfied by different d -spacing in polycrystalline materials. Plotting the angular positions and intensities of the resultant diffracted peaks of radiation produces a pattern, which is characteristic of the sample (fingerprint). Where a mixture of different phases is present, the resulting diffractogram is formed by the addition of the individual patterns. Based on the principle of X-ray diffraction, a wealth of structural, physical and chemical information about the material investigated can be generated.

For a given λ of incident X-rays and inter-planar spacing, d , in a mineral, only specific θ angles will satisfy the Bragg equation. No "reflections" will occur until the incident beam makes an angle θ that satisfies the Bragg equation with $n = 1$. Continued rotation leads to other "reflections" at higher values of θ and when $n = 2, 3$, etc.; these are known as 1st, 2nd, 3rd order, etc., "reflections".

Advantages of XRD:

- Precise phase determination of solid materials
- The X-ray spectra generated provide a structural fingerprint of the known/unknown material.
- Determination of material characteristic such as structure, phase, defects, etc.
- Highest quality and reproducibility of the results.
- Crystallite size can be calculated using Scherer's formula given as

$$T = \frac{K \lambda}{\beta \cos\theta} \quad \text{-----} [2.14]$$

Where, T - crystallite size,

K - a constant,

β - full width at half maximum (FWHM) of the diffraction peak

θ - the angle of reflection.

Even though powder diffraction is the most commonly used technique, there are other versions of XRD that are used for the characterization of materials. They are as follows:

- Single-crystal X-ray diffraction is a technique used to solve the complete structure of crystalline materials, ranging from simple inorganic solids to complex macromolecules, such as proteins.
- Powder diffraction (XRD) is a technique used to characterize the crystallographic structure, crystallite size (grain size), and preferred orientation in polycrystalline or powdered solid samples. Powder diffraction is commonly used to identify unknown substances, by comparing diffraction data against a database maintained by the International Centre for Diffraction Data. It may also be used to characterize heterogeneous solid mixtures to determine the relative abundance of crystalline compounds and, when coupled with lattice refinement techniques, such as Rietveld refinement, can provide structural information on unknown materials. Powder diffraction is also a common method for determining strains in crystalline materials. An effect of the finite crystallite sizes is seen as a broadening of the peaks in X-ray diffraction as is explained by the Scherrer Equation.
- Thin film diffraction and grazing incidence X-ray diffraction may be used to characterize the crystallographic structure and preferred orientation of substrate-anchored thin films.
- High-resolution X-ray diffraction is used to characterize thickness, crystallographic structure, and strain in thin epitaxial films. It employs parallel beam optics [170].
- X-ray pole figure analysis enables one to analyze and determine the distribution of crystalline orientations within a crystalline thin-film sample.
- X-ray rocking curve analysis is used to quantify grain size and mosaic spread in crystalline materials.
- Small angle X-ray scattering (SAXS) probes structure in the nanometer to micrometer range by measuring scattering intensity at scattering angle 2θ close to 0° [171].
- Wide-angle X-ray diffraction (WAXD) can provide information on the quality, amount and arrangement conditions of the crystals. It is often used to determine the crystalline structure of polymers. This technique specifically refers to the analysis of Bragg peaks scattered to wide

angles, which (by Bragg's law) implies that they are caused by sub-nanometer-sized structures. Wide-angle X-ray scattering is the same technique as small-angle X-ray scattering (SAXS) only the distance from the sample to the detector is shorter, and thus diffraction maxima at larger angles are observed [172].

2.4.2.2 Raman spectroscopy

Raman spectroscopy is a spectroscopic technique used to study vibrational, rotational, and other low-frequency modes in a system [173]. It relies on inelastic scattering, or Raman scattering, of monochromatic light, usually from a laser in the visible, near infrared, or near ultraviolet range. The laser light interacts with phonons or other excitations in the system, resulting in the energy of the laser photons being shifted up or down. The shift in energy gives information about the phonon modes in the system. Infrared spectroscopy yields similar, but complementary, information. When a sample is illuminated with a monochromatic light, electrons are excited from the ground state to a virtual energy state and then relax. There are three subsequent possibilities as shown in figure 2.17 [174].

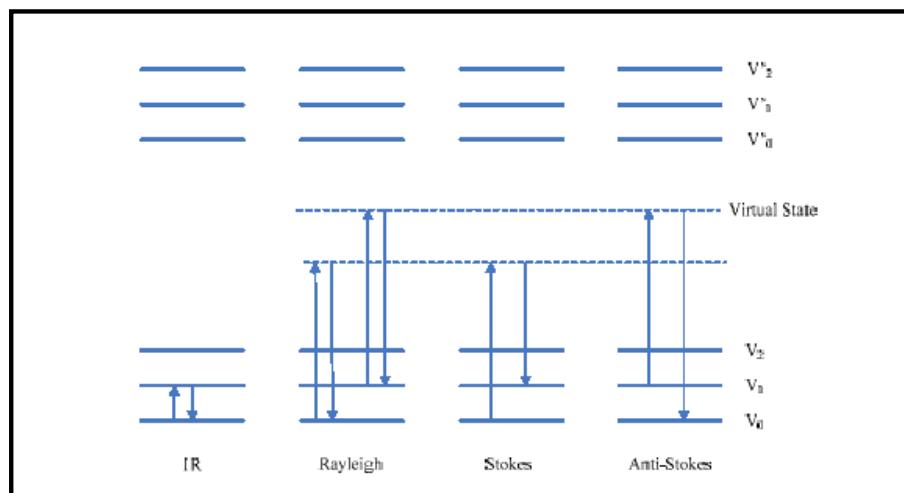


Figure 2.17 Energy level diagram for infrared absorbance, Rayleigh scattering, Stokes Raman scattering and Anti-Stokes Raman scattering [174].

Typically, a sample is illuminated with a laser beam. Light from the illuminated spot is collected with a lens and sent through a monochromator. Wavelengths close to the laser line, due to elastic Rayleigh scattering, are filtered out while the rest of the collected light is dispersed onto a detector.

Variations

Several variations of Raman spectroscopy have been developed. The usual purpose is to enhance the sensitivity (e.g., surface-enhanced Raman), to

improve the spatial resolution (Raman microscopy), or to acquire very specific information (resonance Raman).

- Surface Enhanced Raman Spectroscopy (SERS)
- Resonance Raman spectroscopy
- Surface-Enhanced Resonance Raman Spectroscopy (SERRS)
- Hyper-Raman
- Spontaneous Raman Spectroscopy
- Optical Tweezers Raman Spectroscopy (OTRS)
- Stimulated Raman Spectroscopy
- Spatially Offset Raman Spectroscopy (SORS)
- Coherent anti-Stokes Raman spectroscopy (CARS)
- Raman optical activity (ROA)
- Transmission Raman
- Inverse Raman spectroscopy.
- Tip-Enhanced Raman Spectroscopy (TERS)

Raman spectroscopy has turned out to be a crucial tool for structural characterization of many crystalline materials. It is a complimentary technique to Fourier transform infrared (FTIR) spectroscopy.

2.4.2.3 UV-visible spectroscopy

Ultraviolet-visible spectroscopy (UV = 200 - 400 nm, visible = 400 - 800 nm) corresponds to electronic excitations between the energy levels that correspond to the molecular orbitals on the band gaps of the systems.

Ultraviolet-visible spectroscopy or ultraviolet-visible spectrophotometry (UV-Vis or UV/Vis) refers to absorption spectroscopy or reflectance spectroscopy in the ultraviolet-visible spectral region. This means it uses light in the visible and adjacent (near-UV and near-infrared (NIR)) ranges. The absorption or reflectance in the visible range directly affects the perceived color of the chemicals involved. In this region of the electromagnetic spectrum, molecules undergo electronic transitions. This technique is complementary to fluorescence spectroscopy, in that fluorescence deals with transitions from the excited state to the ground state, while absorption measures transitions from the ground state to the excited state.

The instrument used in UV-vis spectroscopy is called a UV/Vis spectrophotometer. It measures the intensity of light passing through a sample (I), and compares it to the intensity of light before it passes through the sample (I_0). The ratio I / I_0 is called the transmittance and is usually

expressed as a percentage (%T). The absorbance, A , is based on the transmittance (equation 2.15):

$$A = -\log (\%T / 100\%) \quad \text{-----}[2.15]$$

The UV-visible spectrophotometer can also be configured to measure reflectance. In this case, the spectrophotometer measures the intensity of light reflected from a sample (I) and compares it to the intensity of light reflected from a reference material (I_0)(such as a white tile). The ratio I / I_0 is called the reflectance and is usually expressed as a percentage (%R).

Essential parts of a spectrophotometer are a light source, a holder for the sample, a diffraction grating in a monochromator or a prism to separate the different wavelengths of light, and a detector (figure 2.18). The radiation source is often a tungsten filament (300-2500 nm), a deuterium arc lamp, which is continuous over the ultraviolet region (190-400 nm), Xenon arc lamps, which is continuous from 160-2,000 nm; or more recently, light emitting diodes (LED) for the visible wavelengths. The detector is typically a photomultiplier tube, a photodiode, a photodiode array or a charge-coupled device (CCD). Single photodiode detectors and photomultiplier tubes are used with scanning monochromators, which filter the light so that only light of a single wavelength reaches the detector at one time. The scanning monochromator moves the diffraction grating to "step-through" each wavelength so that its intensity may be measured as a function of wavelength. Fixed monochromators are used with CCDs and photodiode arrays. As both of these devices consist of many detectors grouped into one or two-dimensional arrays, they can collect light of different wavelengths on different pixels or groups of pixels simultaneously.

The wavelengths of absorption peaks can be correlated with the types of bonds in a given molecule and are valuable in determining the functional groups within a molecule.

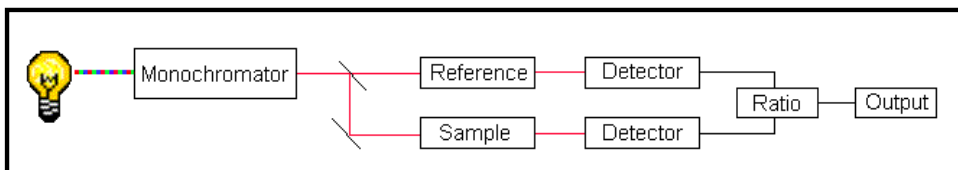


Figure 2.18 Schematic diagram of a double-beam UV-Vis. Spectrophotometer [175].

Penetration depths of electromagnetic radiation are on the order of 50 nm through most of the optical spectrum (visible light). Such small penetration depths limit the applications of optical absorption spectroscopy for the optical characterization of the bulk solids; however, this technique is readily

applicable for the characterization of nanostructures and nanomaterials [175]. UV-visible spectroscopy has turned out to be a very useful tool for characterization of absorption of radiation from metallic nanoparticles (which is based on surface plasmon resonance). It is also vital means of calculating the band gap of semiconductor nanoparticles.

2.4.2.4 X-ray photoelectron spectroscopy

X-ray Photoelectron Spectroscopy (XPS), popularly known as Electron Spectroscopy for Chemical Analysis (ESCA), was developed by K. Siegbahn [168]. The technique is based on the photoelectric effect, as explained by Einstein in 1905. Accordingly (figure 2.19.), photon of fixed energy $h\nu$ incident on an atom ejects an electron of binding energy E_B with kinetic energy E_K according to the equation 2.16

$$h\nu = E_k + E_B \quad \text{-----}[2.16]$$

Knowing $h\nu$ and by measuring with an energy analyzer, the kinetic energy E_K of the electron, the binding energy of an electron in an atom can be determined. The equation is valid for atoms in gasses, liquids or solids. In a solid (see figure 2.20), additional energy (Φ) which is known as the work function of the solid is required for the electron to get emitted as

$$h\nu = E_k + E_B + \Phi \quad \text{-----}[2.17]$$

The work function of solids changes from material to material. It also depends on their cleanliness and purity. Fortunately, it is not necessary to know Φ of the solid. Kinetic energies of emitted electrons are measured with reference to Fermi level, and Φ can be replaced by Φ_{SP} , the work function of the spectrometer. Therefore, one gets the measured E_K , which differs from the kinetic energy of photoelectron coming out from the sample.

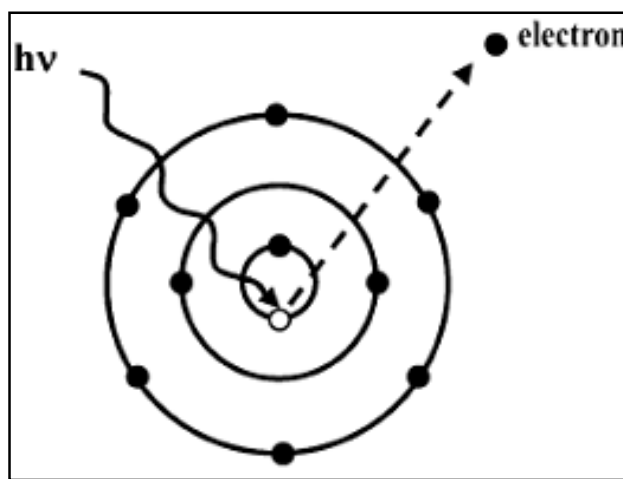


Figure 2.19 Schematic of photoemission [168].

When Fermi level of the sample and the analyzer are aligned (by keeping both at earth potential), there is a constant difference between measured kinetic energy and the kinetic energies of electrons emitted from different samples. As the work function of the spectrometer is known, it is not necessary to know the work function of the samples, and one can easily find out the kinetic or binding energies of the samples.

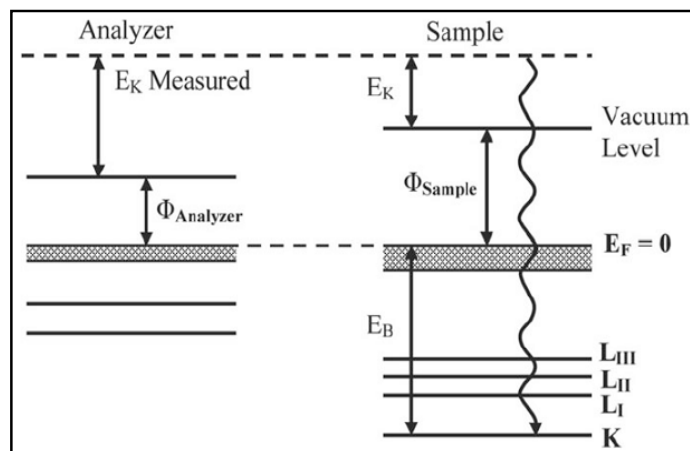


Figure 2.20 Energy level diagram for photoelectron spectroscopy of solids [168].

When an electron is ejected from a solid sample, a hole is created. Binding energy measured, therefore, gives the energy of the photoelectron in the presence of the hole. When an electron leaves an atom, remaining electrons of the atom (and even the surrounding atoms) interact with the hole. The interaction energy depends on the atomic number as well as the energy level in which the hole resides. Corresponding relaxation energies can be significant. Thus binding energies measured in an experiment are not the initial state energies of photoelectrons as depicted in equation 2.17. However, measured binding energies are still quite useful as they are characteristic binding energies of a given element. As mentioned earlier, the photoelectrons have energies which are quite sensitive to their local environment. Thus measurement of binding energies results into useful chemical information.

Ingredients of X-ray photoelectron spectra

Photoelectron spectra are usually rich in their contents. Following ingredients can be made use of in understanding the properties of materials.

- (i) Chemical shift
- (ii) Valence band
- (iii) Auger peaks
- (iv) Spin-orbit splitting
- (v) Multiplet splitting

(vi) *Satellites*

(vii) *Plasmon loss*

Details of these features can be found in some review articles on XPS [168].

2.4.2.5 Dynamic light scattering

It is a technique capable of determining the 'hydrodynamic' size of the particles. Hydrodynamic size can be defined for a particle of irregular shape as the effective size of a particle when it is dispersed in a liquid. For spherical particles, the hydrodynamic size is same as the actual particle size with radius say R. Dynamic Light Scattering (DLS) technique is also known by various names like Photon Correlation Spectroscopy (PCS), Quasi-Elastic Scattering, Diffusive Light Scattering, 3-D Dynamic Light Scattering, Beating Spectroscopy, Homodyne Spectroscopy and Intensity Fluctuation Spectroscopy. However, DLS and PCS are the names which are more common in use. The DLS technique, unlike microscopy techniques like SEM, TEM and AFM as discussed previously in this chapter is capable of determining the particle size or size distribution only when the particles are dispersed in some liquid. The technique depends on the intensity fluctuations of visible light scattered from the particles while they make a random Brownian motion in the liquid. It is Rayleigh scattering and size of the particles has to be much smaller than the wavelength of light used as a source. When a beam of intense and monochromatic coherent beam like laser light falls on a small volume of liquid, the scattered light intensity measured by a detector at certain angle θ with respect to the direction of the incident beam depends on the angle θ , the wavelength of light λ and refractive index n of the medium. The scattering vector value is given as

$$q = \frac{4\pi n}{\lambda} \sin \left(\frac{\theta}{2} \right) \quad \text{-----}[2.18]$$

The scattering geometry is depicted in figure 2.21. If the scattering from each particle occurs only once, the analysis becomes straightforward. Therefore multiple scattering events are avoided using dilute samples or small concentration of particles.

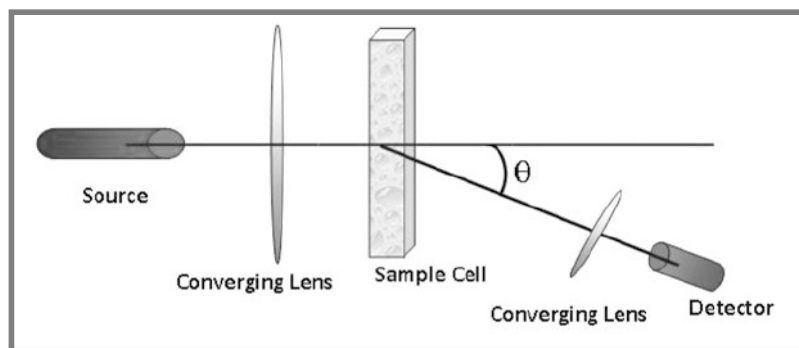


Figure 2.21 Light scattering geometry [168].

In the liquid, it is known from the Stokes-Einstein relation that the diffusion coefficient of particles with radius R is given by

$$D = \frac{kT}{6\pi\eta R} \quad \text{-----[2.19]}$$

Where,

k is Boltzmann constant,

T – temperature of the liquid and

η is the viscosity of the liquid.

As the particles move randomly in the liquid, their scattered intensities at the detector also change randomly or fluctuate. This is because the observed intensity of light from a given volume of liquid depends on the interference of light being scattered from randomly distributed particle of the irradiated volume. The intensity at any instance, therefore, depends upon the relative positions of the particles or phase differences. If the intensity fluctuations due to random motion of particles are analyzed on a time scale smaller than the time taken by the particles to move the distance of the incident wavelength, then one can find that movements of the particles are still correlated. Obviously, if the intensities are measured after a very long time, the positions would not be correlated. When the measurements are made on a very short timescale, the particle position will not change drastically. As more and more time elapses the correlation would become less and less. Correlation decays exponentially. The exponential decay is related to the diffusion of particles and through equation 2.19 to the particle size. If the particles are monodispersed, a single exponential function is expected. Statistical analysis of the intensity fluctuation can be made using the following equation.

$$g^1(t) = \exp(-q^2 D t) \text{-----} [2.20]$$

where, $g^1(t)$ is the first order normalized autocorrelation function, q is the scattering vector length defined by equation 2.20, and D is the diffusion coefficient in the equation. By measuring $g^1(t)$ at one scattering angle, diffusion coefficient (hence particle radius R) of particles can be obtained.

The experimental setup is very simple as schematically shown in figure 2.21 and the commercial instruments are equipped with determining the autocorrelation function including cumulant method (for particles which are not monodispersed). They are able to give information of diffusion coefficients as well as particle size distribution over a wide range of ~1 nm to 10 μm size. Usually, a beam of laser light is necessary, as the concentration of particles in the solution has to be kept low in order to avoid the multiple scattering effects. One also tries to use efficient detectors like avalanche photodiode, so that good signal is obtained.

2.5. Motivation and Scope

Based on the insight obtained from the literature survey it was realized that there is tremendous scope for the research in the field of nanomaterials of the molybdenum family especially metallic molybdenum, molybdenum trioxide and molybdenum disulfide and their nanocomposites. **Considering the discussion in this section particularly regarding the challenges in the synthesis of nanomaterials, our first motivation was to explore appropriate techniques for the synthesis of *functional* nanomaterials of molybdenum family. The second motivation was to explore the applications of synthesized nanomaterials in unfathomed areas of applications which are important scientifically and industrially as well as to the society *at large*.**

In order to accomplish the first motivation, the following strategy has been evolved:

- (i) ***Synthesis of plain and hierarchical nanostructures of Mo and MoS₂ by a conventional solvothermal route which is not explored in detail till date.***
- (ii) ***Rapid generation of MoS₂ nanostructures via microwave assisted solvothermal route.*** To the best of our knowledge, this technique has not been reported for the synthesis of MoS₂ nanostructures.

- (iii) **Large scale production of nanocomposites of Mo-MoO₃-PPS and MoO₃ –PPS using facile, economical and green solid-solid reaction route.** To our finest understanding, this technique has not been reported for generation of nanocomposites of these products.
- (iv) **Gram-scale production of MoO₃ nanostructures using facile, economical conventional and ultrasonication assisted sol-gel reaction route.** To the best of our knowledge, there are no reports pertaining to the synthesis of MoO₃ nanostructures using conventional and ultrasonication assisted sol-gel route.

Strategy planned to fulfill the second motivation deals with

- (i) **Exploration of antimicrobial as well as biofilm inhibition activity of MoS₂ nanostructures as well as nanocomposites of Mo-MoO₃-PPS**
- (ii) **Investigation on achieving superior dielectric constant in nanocomposites of MoO₃ –PPS as a step towards their high-temperature capacitor application.**
- (iii) **Examination of photocatalytic activities of MoO₃ nanostructures prepared by sol-gel (conventional and ultrasonic assisted) as well as solid-solid state reaction methods.**

The details corresponding to the actual experimental work carried out corresponding to the above strategies are presented in chapter 3, 4 and 5, respectively. The *salient features* of these chapters include:

- a) *Detailed description of the experimental work related to the synthesis of nanoscale materials.*
- b) *Discussion of the results based on the physicochemical characterization.*
- c) *Exploration of the application-oriented work for some of the synthesized nanomaterials.*

The overall conclusions of the work along with the significant research findings accomplished in this thesis are presented in Chapter 6. Scope for the further future work is also discussed in the same chapter.

Digest of the *main objectives* of the present thesis work are:

- 1) *Synthesis of MoS₂ nanostructures using conventional and microwave assisted solvothermal techniques.*
- 2) *Synthesis of nanostructured Mo-MoO₃-PPS as well as MoO₃-PPS based nanocomposites in thermally stable polyphenylenesulphide (PPS) polymer matrix.*

-
- 3) *Synthesis of MoO₃ nanostructures using conventional and ultrasonication (sonochemical) assisted sol-gel routes.*
 - 4) *Study the nanocomposites and nanostructures for crystallographic, morphological, optical, thermal and magnetic properties by various physicochemical characterization techniques.*
 - 5) *Exploration of applications of synthesized nanocomposites and nanostructures in territories like photocatalysis, bioscience, and electronics.*

References

- [1] Cushing. B. L., Kolesnichenko V. L. and Connor C. J. O. (2004) "Recent advances in the liquid-phase syntheses of inorganic nanoparticles" *Chem. Rev.* 104: 3893.
- [2] Swihart. M. T. (2003) "Vapor-phase synthesis of nanoparticles" *Curr. Opin. Colloid Interface Sci.*8:127–133.
- [3] Masala. O. and Seshadri. R. (2004) "Synthesis routes for large volumes of nanoparticles" *Annu. Rev. Mater. Res.*34:41–81.
- [4] Burda. C., Chen X., Narayanan. R. and El-Sayed M. A. (2005) "Chemistry and Properties of Nanocrystals of Different Shapes" *Chem. Rev.* 105: 1025.
- [5] Byrappa. K. and Yoshimura. M. (2001) "Handbook of Hydrothermal Technology" Noyes Publications, New Jersey, USA.
- [6] Lee J. W., Hall A. S., Kim J. D. and Mallouk T. E. (2012) "A Facile and Template Free Hydrothermal Synthesis of Mn₃O₄ Nanorods on Graphene Sheets for Supercapacitor Electrodes with Long Cycle Stability" *Chem. Mater.* 24 (6):1158–1164.
- [7] Wan. H., Ji X., Jiang J., Yu J., Miao L., Zhang L., Bie S., Chen H. and Ruan Y. (2013) "Hydrothermal synthesis of cobalt sulfide nanotubes: The size control and its application in supercapacitors" *Journal of Power Sources* 243:396–402.
- [8] Yu. M. Y., Cui D. L., Kai L., Yin Y. S., Wang Q. L. and Lei C. (2005) "Hydrothermal synthesis of cubic boron nitride crystals" *Mater. Sci. Engg. B* 121: 166–169.
- [9] Shinde. M. D., Chavan P. G., Umarji G. G., Arbuji S. S., Rane S. B., More M. A., Joag D. S. and Amalnerkar D. P. (2012) "Field emission and photo-catalytic investigations on hierarchical nanostructures of copper doped CdS synthesized by kitchen-chemistry approach" *J. Nanosci. Nanotechnol.* 12: 3788-3798.
- [10] Zawadzki M. (2012) "Preparation and characterization of ceria nanoparticles by microwave-assisted solvothermal process" *J. Nanosci. Nanotechnol.*12:3788-3798.
- [11] Sutton W. H. (1993) "Key issues in microwave process technology" *Ceramic transactions: Microwaves. Theory and application in materials processing II*:36.
- [12] Gabriel C., Gabriel S., Grant E. H., Halstead S. J. and Mingos D. M. P. (1998) "Dielectric parameters relevant to microwave dielectric heating" *Chem. Soc. Rev.* 27:213-224.
- [13] Rao K. J., Vaidhyanathan B., Ganguli M., and Ramakrishnan P. A. (1999) "Synthesis of inorganic solids using microwaves" *Chem. Mater.* 11: 882.

-
- [14] Senise J. T. and Jermolovicius L. A. (2004) "Microwave Chemistry – a fertile field for scientific research and industrial applications" *J. Microwaves and Optoelectron* 3: 97-112.
- [15] Anamin group (2010) <http://www.anamingroup.cl/digestor-de-muestra/>.
- [16] Komarneni S. and Katsuki H. (2002) "Nanophase materials by a novel microwave hydrothermal process" *Pure Appl. Chem.* 74:1537- 1543.
- [17] Michael D., Mingos P. and Baghurst D. R. (1991) "Tilden lecture applications of microwave dielectric heating effects to synthetic problems in chemistry" *Chem. Soc. Rev.* 20:1-47.
- [18] Shi S. and Hwang J. Y. (2003) "Microwave-assisted wet chemical synthesis: advantages, significance, and steps to industrialization" *J. Minerals Mater. Char. Engg.* 2:101-110.
- [19] Clark D. E. and Sutton W. H. (1996) "Microwave processing of materials" *Ann. Rev. Mater. Sci.* 26: 299-331.
- [20] Muster J., Kim G. T., Krstic V., Park J. G., Park Y. W., Roth S., and Burghard M. (2000) "Electrical transport through individual vanadium pentoxide nanowires" *Adv. Mater.* 12: 420-424.
- [21] Liu X., Pan L., Lv T., Zhu G., Sun Z. and Sun C. (2011) "Microwave-assisted synthesis of CdS-reduced graphene oxide composites for photocatalytic reduction of Cr(VI)" *Chem. Commun.* 47: 11984 -11986.
- [22] Krishnakumar T., P. Nicola, Prasanna Kumari K., Perumal K. and Jayaprakash R. (2008) "Microwave-assisted synthesis and characterization of tin oxide nanoparticles" *Mater. Lett.* 62: 3437–3440.
- [23] Corradi A. B., Bondioli F. and Focher B. (2005) "Conventional and Microwave-hydrothermal synthesis of TiO₂ nanopowders" *J. Am. Ceram. Soc.* 88: 2639–2641.
- [24] Wang W. W., Zhu Y. J. and Ruan M. L. (2007) "Microwave-assisted synthesis and magnetic property of magnetite and hematite nanoparticles" *J. Nanopart. Res.* 9: 419–426.
- [25] Yang H., Huang C., Tang A., Zhang X. and Yang W. (2005) "Microwave-assisted synthesis of ceria nanoparticles" *Mater. Res. Bull.* 40:1690–1695.
- [26] Yang H., Huang C., Su X. and Tang A. (2005) "Microwave-assisted synthesis and luminescent properties of pure and doped ZnS nanoparticles" *J. Alloys and Compounds* 402: 274–277.
- [27] Barreto G., Morales G., Cañizo A. and Eyler N. (2015) "Microwave assisted synthesis of ZnO tridimensional nanostructures" *Mater. Sci.* 8: 535-540.

- [28] Tsuji M., Hashimoto M., Nishizaw Y., Kubokaw M. and Tsuji T. (2005) "Microwave-assisted synthesis of metallic nanostructures in solution" Chem. Eur. J. 11: 440–452
- [29] Makhluf S., Dror R., Nitzan Y., Abramovich Y., Jelinek R. and Gedanken A. (2005) "Microwave-assisted synthesis of nanocrystalline MgO and its use as a bactericide" Adv. Fun. Mater. 15:1708–1715.
- [30] Chena S. Q. and Wang Y. (2010) "Microwave-assisted synthesis of a Co₃O₄-graphene sheet-on-sheet nanocomposite as a superior anode material for Li-ion batteries" J. Mater. Chem. 20:9735-9739.
- [31] Bradly D. (2002) "Nano the hedgehog": The Alchemist, News Research Chemistry in Britain: 42. <http://www.rsc.org/suppdata/jm/b5/b503285g/b503285g.pdf>
- [32] Schubert U. and Husing N. (2009) "Synthesis of inorganic materials" Wiley-VCH ISBN: 3-527-29550-X. Second edition and third, completely revised and updated edition (2012), ISBN 3-527-32714-0.
- [33] Fan H. J., Knez M., Scholz R., Hesse D., Nielsch K., Zacharias M. and Gosele U. (2007) "Influence of surface diffusion on the formation of hollow nanostructures induced by the Kirkendall effect: the basic concept" Nano Lett. 7: 993-997.
- [34] Liu Y. L., Liu Z. M., Yang Y., Yang H. F., Shen G. L. and Yu R. Q. (2005) "Simple synthesis of MgFe₂O₄ nanoparticles as gas sensing materials" Sens. Actuator B-Chem. 107: 600–604.
- [35] Sun Z. P., Liu L., Zhang L. and Jia D. Z. (2006) "Rapid synthesis of ZnO nanorods by one-step, room-temperature, solid-state reaction and their gas-sensing properties" Nanotechnology 17: 2266.
- [36] Choi D., Wang D., Bae I. T., Xiao J., Nie Z., Wang W., Viswanathan V. V., Lee Y. J., Zhang J. G., Graff G. L., Yang Z. and Liu J. (2010) "LiMnPO₄ nanoplate grown via solid-state reaction in molten hydrocarbon for Li-ion battery cathode" Nano Lett. 10: 2799–2805.
- [37] Wang W., Liu Y., Zhan Y., Zheng C. and Wang G. (2001) "A novel and simple one-step solid-state reaction for the synthesis of PbS nanoparticles in the presence of a suitable surfactant" Mater. Res. Bull. 36: 1977–1984.
- [38] Yang H., Tao Q., Zhang X., Tang A. and Ouyang J. (2008) "Solid-state synthesis and electrochemical property of SnO₂/NiO nanomaterials" J. of Alloys and Compounds 459: 98–102.

- [39] Cao Y., Jia D., Zhou J. and Sun Y. (2009) "simple solid-state chemical synthesis of ZnSnO₃ nanocubes and their application as gas sensors" *Eur. J. Inorg. Chem.* 4105–4109.
- [40] Liu S. Y., Tang Q. L. and Feng Q. G. (2011) "Synthesis of S/Cr doped mesoporous TiO₂ with high-active visible light degradation property via solid state reaction route" *Appl. Surf. Sci.* 257: 5544–5551.
- [41] Li F., Yu X., Pan H., Wang M. and Xin X. (2000) "Syntheses of MO₂ (M=Si, Ce, Sn) nanoparticles by solid-state reactions at ambient temperature" *Solid State Sci.* 2: 767–772.
- [42] Li F., Chen L., Chen Z., Xu J., Zhu J. and Xin X. (2002) "Two-step solid-state synthesis of tin oxide and its gas-sensing property" *Mater. Chem. Phys.* 73: 335–338.
- [43] Qureshi N., Umarji G., Shinde M., Rane V., Borde L., Mulik U. and Amalnerkar D. (2013) "Innate approach for fabrication of nickel oxide nanocomposite in pellet form and their electric properties" *Mater. Exp.* 3:79-84.
- [44] Wang W., Liu Z., Zheng C., Xu C., Liu Y. and Wang G. (2003) "Synthesis of CdS nanoparticles by a novel and simple one-step, solid-state reaction in the presence of a nonionic surfactant" *Mater. Lett.* 57: 2755 – 2760.
- [45] Waghmare S., Shinde M., Gholap R., Rao N. K., Hawaldar R., Mulik U. and Amalnerkar D. (2009) "Concurrent in-situ formation of Ag / Ag₂S nanoparticles in polymer matrix by facile polymer-inorganic solid state reaction" *J. Nano Res.* 5: 143-152.
- [46] Rumale N., Arbuj S., Umarji G., Shinde M., Mulik U., Pokle A., Shinde S. and Amalnerkar D. (2013) "In-situ fabrication of cobalt oxide/sulphide mixed phase nanoparticles in Polyphenylenesulphide matrix" *Carb. Sci. Tech.* 5:236 – 243.
- [47] Waghmare S., Adhyapak P., Shinde M., Gholap R., Mulik U. and Amalnerkar D. (2011) "One-pot synthesis of semiconducting PbS nanorods within poly(phenylene sulphide) matrix" *J. Nanosci. Nanotech.* 11: 5098-5101.
- [48] Rumale N., Arbuj S., Umarji G., Shinde M., Mulik U., Pokle A. and Amalnerkar D. (2013) "Simplistic approach for in-situ generation of ZnS quantum dots in polyphenylene sulphide matrix via chalcogen enriched solid-solid reaction technique" *Phys.Status Solid A* 210: 345-348.
- [49] L. L. Hench and J. K. West (1990) "The sol-gel process" *Chem. Rev.* 90:33-72.
- [50] Aravindan V., Karthikeyan K., Ravi S., Amaresh S., Kim W. S. and Lee Y. S. (2010) "Adipic acid assisted sol-gel synthesis of Li₂MnSiO₄ nanoparticles with improved lithium storage properties" *J. Mater. Chem.* 20:7340–7343.

-
- [51] Lu Y., Yin Y., Mayers B. T., and Xia Y. (2002) "Modifying the surface properties of superparamagnetic iron oxide nanoparticles through a sol-gel approach" *Nano Lett.* 2:183-186.
- [52] Ennas G., Musinu A., Piccalug G. and Zedda D. (1998) "Characterization of iron oxide nanoparticles in an Fe₂O₃-SiO₂ composite prepared by a sol-gel method" *Chem. Mater.* 10: 495-502.
- [53] Xu J., Yang H., Fu W., Du K., Sui Y., Chen J., Zeng Y., Li M. and Zou G. (2007) "Preparation and magnetic properties of magnetite nanoparticles by sol-gel method" *J. Magne. Magnet. Mater.* 309:307-311.
- [54] Vafae M. and Ghamsari M. S. (2007) "Preparation and characterization of ZnO nanoparticles by a novel sol-gel route" *Mater. Lett.* 61: 3265-3268.
- [55] Tang J., Fabbri J., Robinson R. D., Zhu Y., Herman I. P., Steigerwald M. L. and Brus L. E. (2004) "Solid-solution nanoparticles: use of a nonhydrolytic sol-gel synthesis to prepare HfO₂ and Hf_xZr_{1-x}O₂ nanocrystals" *Chem. Mater.* 16:1336-1342.
- [56] Thota S. and Kumar J. (2007) "Sol-gel synthesis and anomalous magnetic behavior of NiO nanoparticles" *J. Phys. Chem. Soli.* 68:1951-1964.
- [57] Cao H., Xu Y., Hong J., Liu H., Yin G., Li B., Tie C. and Xu Z. (2001) "Sol-gel template synthesis of an array of single crystal CdS nanowires on a porous alumina template" *Adv. Mater.* 13:1393-1394.
- [58] Devarajan S., Bera P. and Sampath S. (2005) "Bimetallic nanoparticles: a single step synthesis, stabilization, and characterization of Au-Ag, Au-Pd, and Au-Pt in sol-gel derived silicates" *J. Coll. Interf. Sci.* 290:117-129.
- [59] Woo K., Lee H. J., Ahn J. P. and Park Y. S. (2003) "Sol-gel mediated synthesis of Fe₂O₃ Nanorods" *Adv. Mater.* 15: 1761-1764.
- [60] Prasad K., Pinjari D.V., Pandit A. B. and Mhaske S. T. (2010) "Phase transformation of nanostructured titanium dioxide from anatase-to-rutile via combined ultrasound assisted sol-gel technique" *Ultrason. Sonochem.* 17: 409-415.
- [61] Gedanken A. (2004) "Using sonochemistry for the fabrication of nanomaterials" *Ultrason. Sonochem.* 11:47-55.
- [62] Patil M. N. and Pandit A. B. (2007) "Cavitation – a novel technique for making stable nanosuspensions" *Ultrason. Sonochem.* 14: 519-530.
- [63] Afanasiev P. (2008) "Synthetic approaches to the molybdenum sulfide materials" *C. R. Chimie.* 11: 159-182.

- [64] Maia L, Yang F, Zhao Y., Xu X., Xu L., Hu B., Luo Y. and Liu H. (2011) "Molybdenum oxide nanowires: synthesis & properties" *Mater. Today* 14:346-353.
- [65] <http://www.comparisonofmetals.com/en/what-is-molybdenum/model-34-0>
- [66] Siddiqui M. A., Saquib Q., Ahamed M., Farshorid N. N., Ahmad J., Wahab R., Khan S. T., Alhadlaq H. A., Musarrat J., Al-Khedhairy A. A. and Pant A. B. (2015) "Molybdenum nanoparticles-induced cytotoxicity, oxidative stress, G2/M arrest, and DNA damage in mouse skin fibroblast cells (L929)" *Colloi. Surf. B: Biointerf.* 125: 73–81.
- [67] Howalt J. G. and Vegge T. (2014) "The role of oxygen and water on molybdenum nanoclusters for electro catalytic ammonia production" *Beilstein J. Nanotechnol.* 5: 111–120.
- [68] Zhou J., Xu N. S., Dong S. Z., Chen J., She J. C. and Wang Z. L. (2014) "Large are nanowires arrays of Mo/MoO: synthesis and field emission properties" *Adv. Mater.* 15 :1835-1840.
- [69] Taran L. N. Y., Gonchar O. M., Lopatko K. G., Batsmanova L. M., Patyka M. V. and Volkogon M. V. (2014) "The effect of colloidal solution of molybdenum nanoparticles on the microbial composition in rhizosphere of cicer arietinum" *Nanoscale Res. Lett.*9: 289.
- [70] Mohanty B., Morton B. D., Alagoz A. S., Karabacak T. and Zou M. (2014) "Frictional anisotropy of tilted molybdenum nanorods fabricated by glancing angle deposition" *Tribo. Internat.* 80:216–221.
- [71] Shpak A. P., Kotrechko S. O., Mazilova T. I. and Mikhailovskij I. M. (2009) "Inherent tensile strength of molybdenum nanocrystals" *Sci. Tech. Adv. Mater* 10: 045004 (9).
- [72] Mandal S. and Ahiri S. (2012) "Synthesis of molybdenum nanoparticles by in-situ γ -radiation" *Appl. Radi. Isoto.* 70: 2340–2343.
- [73] Park J. I. (2011) "Chapter 3: Nanoparticle synthesis & applications synthesis of molybdenum nanoparticles by RF plasma advanced materials, CNTs, particles, films and composites" *Nanotech.* 271 – 273.
- [74] Potapenko D. V., Horna J. M., Beuhler R. J., Song Z. and Michael G. (2005) "Reactivity studies with gold-supported molybdenum nanoparticles" *White Surf. Sci.* 574: 244–258.
- [75] Purohit V. S., Bhise A. B., Deya S., More M. A., Dharmadhikari C. V., Joag D. S., Pasrich R. and Bhoraskar S.V. (2008) "Scanning tunneling microscopic and field emission microscopic studies of nanostructured molybdenum film synthesized by electron cyclotron resonance plasma" *Vacuum* 83: 435–443.

- [76] Chen L., Lu T. M and Wang G. C. (2011) "Biaxially textured Mo films with diverse morphologies by substrate-flipping rotation" *Nanotech.* 22: 505701.
- [77] Giovanni M. and Pumera M. (2011) "Molybdenum metallic nanoparticle detection via differential pulse voltammetry" *Electrochem. Comm.* 13: 203–204.
- [78] Chang L., Yang H., Li J., Fu W., Du Y., Du K., Yu Q., Xu J. and Li M., (2006) "Simple synthesis and characteristics of Mo/MoS₂ inorganic fullerene-like and actinomorphic nanospheres with core-shell structure" *Nanotech.* 17: 3827–3831.
- [79] Park J. C. and Song H. (2007) "Synthesis of polycrystalline Mo/MoO_x nanoflakes and their transformation to MoO₃ and MoS₂ nanoparticles" *Chem.Mater.* 19:2706-2708.
- [80] Ramana C. V., Atuchin V. V., Troitskaia I. B., Gromilov S. A., Kostrovsky V. G. and Saupe G. B. (2009) "Low-temperature synthesis of morphology controlled metastable hexagonal molybdenum trioxide (MoO₃)" *Solid State Comm.* 149:6-9.
- [81] Shi Y., Guo B., Corr S. A., Shi Q., Hu Y. S., Heier K. R., Chen L., Seshadri R. and Stucky G. D. (2009) "Ordered mesoporous metallic MoO₂ materials with highly reversible lithium storage capacity" *Nano Lett.* 9: 4215.
- [82] Song J., Wang X., Ni X., Zheng H., Zhang Z., Ji M., Shen T. and Wang X. (2005) "Preparation of hexagonal-MoO₃ and electrochemical properties of lithium intercalation into the oxide" *Mater. Res. Bull.* 40: 1751–1756.
- [83] Mai L., Hu B., Qi Y., Dai Y. and Chen W (2008) "Improved cycling performance of directly lithiated MoO₃ nanobelts" *Int. J. Electrochem. Sci.* 3: 216-222.
- [84] Ding Y., Wan Y., Min Y. L., Zhang W. and Yu S. H. (2008) "General synthesis and phase control of metal molybdate hydrates MMoO₄·nH₂O (M = Co, Ni, Mn, n = 0, 3/4, 1) nano/microcrystals by a hydrothermal approach: magnetic, photocatalytic, and electrochemical properties" *Inorg. Chem.* 47:7813–7823.
- [85] Sharma N., Shaju K. M., Subba Rao G. V., Chowdari B. V. R., Dong Z. L. and White T. J. (2003) "Carbon-coated nanophase CaMoO₄ as anode material for li-ion batteries" *Chem. Mater.* 16: 504–512.
- [86] Chithambararaj A., Sanjini N. S., Velmathi S. and Chandra Bose A. (2013) "Preparation of h-MoO₃ and α-MoO₃ nanocrystals: comparative study on photocatalytic degradation of methylene blue under visible light irradiation" *Phys. Chem.* 15:14761.
- [87] Liang R., Cao H. and Qian D. (2011) "MoO₃ nanowires as electrochemical pseudocapacitor materials" *Chem. Commun.* 47: 10305–10307.

- [88] Zhou J., Xu N. S., Deng S. Z., Chen J., She J. C. and Wang Z. L. (2003) "Large-area nanowire arrays of molybdenum and molybdenum oxides: synthesis and field emission properties" *Adv. Mater.* 15:1835–1840.
- [89] Kim W. S., Kim H. C. and Seong-Hyeon. (2010) "Hong Gas sensing properties of MoO₃ nanoparticles synthesized by solvothermal method" *J. Nanopart. Res.* 12:1889–1896.
- [90] Barazzouk S., Tandon R. P. and Hotchandani S. (2006) "MoO₃-based sensor for NO, NO₂ and CH₄ detection" *Sens. Actuat. B.* 119:691–694.
- [91] Sunu S. S., Prabhu E., Jayaraman V., Gnanasekar K. I. and Gnanasekaran T. (2003) "Gas sensing properties of PLD made MoO₃ films" *Sens. Actuat. B.* 94:189–196.
- [92] Imawan C., Steffes H. and Obermeier S. F. (2001) "A new preparation method for sputtered MoO₃ multilayers for the application in gas sensors" *Sens. Actuat. B.* 78:119–125.
- [93] Stubhan T., Ameri T., Salinas M., Krantz J., Machui F., Halik M., and Brabec C. J. (2011) "High shunt resistance in polymer solar cells comprising a MoO₃ hole extraction layer processed from nanoparticle suspension" *Appl. Phys. Lett.* 98, 253: 308.
- [94] Jasieniak J. J., Seifert J., Jang J., Mates T. and Heeger A. J. (2012) "A solution-processed MoO_x anode interlayer for use within organic photovoltaic devices" *Adv. Funct. Mater.* 22:2594–2605.
- [95] http://en.wikipedia.org/wiki/Molybdenum_trioxide
- [96] Uttam K. S. and Mitra S. (2012) "Electrochemical activity of α-MoO₃ nano-belts as lithium-ion battery cathode" *RSC Adv.* 2: 11123-11131.
- [97] Chithambararaj A., Winston B., Sanjini N. S., Velmathi S. and Bose A. C. (2015) "Band gap tuning of h-MoO₃ nanocrystals for efficient visible light photocatalytic activity against methylene blue dye" *J. Nanosci. Nanotechnol.* 15(7).
- [98] Fang L., Shu Y., Wang A. and Zhang T. (2007) "Green synthesis and characterization of anisotropic uniform single-crystal α-MoO₃ nanostructures" *J. Phys. Chem. C.* 111:2401–2408.
- [99] Jun S. C., Yan L. C., Srinivasan M. and Xiong W. L. (2010) "Fast synthesis of α-MoO₃ nanorods with controlled aspect ratios and their enhanced lithium storage capabilities" *J. Phys. Chem. C.* 114: 8675–8678.
- [100] Brezesinski T., Wang J., Tolbert S. H. and Dunn B. (2010) "Ordered mesoporous α-MoO₃ with iso-oriented nanocrystalline walls for thin-film pseudocapacitors" *Nature Mater.* 9: 146–151.

- [101] Lou X. W. and Zeng H. C. (2002) "Hydrothermal synthesis of α - MoO_3 nanorods via acidification of ammonium heptamolybdate tetrahydrate" *Chem. Mater.* 14: 4781–4789.
- [102] Cai L., Rao P. M. and Zheng X. (2011) "Morphology-controlled flame synthesis of single, branched, and flower-like α - MoO_3 nanobelt arrays" *Nano Lett.* 11: 872–877.
- [103] Zhiyu W., Srinivasan M and Xiong W. L. (2012) "Ultralong α - MoO_3 nanobelts: synthesis and effect of binder choice on their lithium storage properties" *J. Phys. Chem. C* 116: 12508–12513.
- [104] Sui L., Xu Y. M., Zhang X. F., Cheng X. L., Gao S., Zhao H., Cai Z. and Huo L. H. (2015) "Construction of three-dimensional flower-like α - MoO_3 with hierarchical structure for highly selective triethylamine sensor" *Sens. Actua. B: Chemical* 208: 406–414.
- [105] Zhou L., Yang L., Yuan P., Zou J., Wu Y. and C. Yu. (2010) " α - MoO_3 nanobelts: a high performance cathode material for lithium ion batteries" *J. Phys. Chem. C* 114: 21868–21872.
- [106] Zheng L., Xu Y., Jin D. and Xie Y. (2009) "Novel metastable hexagonal MoO_3 nanobelts: synthesis, photochromic, and electrochromic properties" *Chem. Mater.* 21 (23): 5681–5690.
- [107] Li G., Jiang L., Pang S., Peng H. and Zhang Z. (2006) "Molybdenum trioxide nanostructures: the evolution from helical nanosheets to crosslike nanoflowers to nanobelts" *J. Phys. Chem. B.* 110: 24472–24475.
- [108] Dewangan K., Sinha N. N., Sharma P. K., Pandey A. C., Munichandraiah N. and Gajbhiye N. S. (2011) "Synthesis and characterization of single-crystalline α - MoO_3 nanofibers for enhanced Li-ion intercalation applications" *Cryst. Eng. Comm.* 13: 927-933.
- [109] Yao D. D., Ou J. Z., Latham K., Zhuiykov S., O'Mullane A. P. and Kalantar-zadeh K. (2012) "Electrodeposited α - and β -phase MoO_3 films and investigation of their gasochromic properties" *Cryst. Growth Des.* 12:1865–1870.
- [110] Phuruangrat A., Chen J. S., Lou X. W., Yayapao O., Thongtem S., Thongtem T. (2012) "Hydrothermal synthesis and electrochemical properties of α - MoO_3 nanobelts used as cathode materials for Li-ion batteries" *Appl. Phys. A.* 107: 249-254.
- [111] Xie Y. L., Cheong F. C., Zhu Y. W., Varghese B., Tamang R., Bettiol A. A. and Sow C. H. (2010) "Rainbow-like MoO_3 nanobelts fashioned via AFM micromachining" *J. Phys. Chem. C.* 114:120–124.

- [112] Hosono K., Matsubara I., Murayama N., Woosuck S. and Izu N. (2005) "Synthesis of polypyrrole/MoO₃ hybrid thin films and their volatile organic compound gas-sensing properties" *Chem. Mater.* 17: 349–354.
- [113] Paraguay-Delgado F., Albitar M. A., Huirache-Acuña R., Verde Y., Alonso-Núñez G. (2007) "Optimization of the synthesis of α -MoO₃ nanoribbons and hydrodesulfurization (HDS) catalyst test" *J. Nanosci. Nanotechnol.* 7: 3677-3683.
- [114] Illyaskutty N., Sreedhar S., Kumar G. S., Kohler H., Schwotzer M., Natzeck C. and Pillai V. P. M. (2014) "Alteration of architecture of MoO₃ nanostructures on arbitrary substrates: growth kinetics, spectroscopic and gas sensing properties" *Nanoscale* 6: 13882-13894.
- [115] Ban D., Deng S., Xu N., Chen J., She J. and Liu F. (2010) "Improved field emission characteristics of large-area films of molybdenum trioxide microbelt" *J. Nanomater.* 6.
- [116] Gouma P., Kalyanasundaram K. and Bishop A. (2006) "Electrospun single-crystal MoO₃ nanowires for biochemistry sensing probes" *J. Mater. Res.* 21: 2904-2910.
- [117] O'Hare P. A. G., Benn E., Cheng F. Y. and Kuzmycz G. (1970) "A fluorine bomb calorimetric study of molybdenum disulfide the standard enthalpies of formation of the di- and sesquisulfides of molybdenum" *J. Chem. Thermodyn.* 2: 797.
- [118] Murray R. and Evans B. L. (1979) "The thermal expansion of 2H-MoS₂ and 2H-WSe₂ between 10 and 320 K" *J. Appl. Crystallogr.* 12:312.
- [119] Bell R. E. and Herfert R. E. (1957) "Preparation and characterization of a new crystalline form of MoS₂" *J. Am. Chem. Soc.* 79: 3351-3354.
- [120] Wypych F. and Schok Ilhorn R. (1992) "1T-MoS₂, a new metallic modification of molybdenum disulfide" *J. Chem. Soc. Chem. Commun.* 1386-1388.
- [121] Park K. T., Richards-Babb M., Hess J. S., Weiss J. and Klier K. (1996) "Valence-band electronic structure of MoS₂ and Cs/MoS₂ (0002) studied by angle-resolved x-ray photoemission spectroscopy" *Phys. Rev. B.* 54: 5471.
- [122] Wilson J. A. and Yoffe A. D. (1969) "The transition metal dichalcogenides discussion and interpretation of the observed optical, electrical and structural properties" *Adv. Phys.* 18: 193.
- [123] Jun-Feng Y., Braham P., Jens H. and Qian-Feng F. (2012) "Tribological properties of transition metal di-chalcogenide based lubricant coatings" *Front Mater. Sci.* 6: 116-127.

- [124] Alfred W. N., Charleston W. V., Albert S. Behan and Bronxville N. Y. (1981) United States Patent, Union Carbide Corporation, New York, N.Y: 47:239.
- [125] Splendiani A., Sun L., Zhang Y., Li T., Kim J., Chim C. Y., Galli G. and Wang F. (2010) "Emerging photoluminescence in monolayer MoS₂" Nano Lett. 10: 1271–1275.
- [126] Popov I., Pecchia A., Okano S., Ranjan N., Carlo A. D. and Seifert G. (2008) "Electronic and transport properties of contacts between molybdenum sulfide nanowires and gold electrodes" Appl. Phys. Let. 93: 083115.
- [127] Kam K. K. and Parkinson B. A. (1982) "Detailed photocurrent spectroscopy of the semiconducting group VIB transition metal dichalcogenides" J. Phys. Chem. 86: 463-467.
- [128] Radisavljevic B., Radenovic A., Brivio J., Giacometti V. and Kis A. (2011) "Single layer MoS₂ transistors" Nature Nanotech. 6:147-150.
- [129] Maja R., Ales M., Zora S., Adolf J., Miran C., Jure D., Pierre S., Francis L. and Dragan M. (2001) "Self assembly of sub-nanometer diameter single wall MoS₂ nanotubes" Sci. 292:479-481.
- [130] Feildman Y., Wasserman E., Srolovitz D. J. and Tenne R. (1995) "High rate gas phase growth of MoS₂ nested inorganic fullerenes and nanotubes" Science . 267: 222-225.
- [131] Peng Y., Meng Z., Zhong C., Lu J., Yu W., Jia Y. B. and Qian Y. (2001) "Hydrothermal synthesis and characterization of single-molecular-layer MoS₂ and MoSe₂" Chem. Lett. 772 - 773.
- [132] Wingkei H., Jimmy C. Y., Jun L., Jiaguo Y. and Puishan L. (2004) "Preparation and photocatalytic behavior of MoS₂ and WS₂ nanocluster sensitized TiO₂" Langmuir 20: 5865-5869.
- [133] Chen X., Wang X., Wang Z., Yu W. and Qian Y. (2004) "Direct sulfidization synthesis of high-quality binary sulfides (WS₂, MoS₂, V₅S₈) from the respective oxides" Mater. Chem. Phys. 87: 327-331.
- [134] Xiang Q., Yu J. and Jaroniec M. (2012) "Synergetic effect of MoS₂ and grapheme as cocatalysts for enhanced photocatalytic H₂ production activity of TiO₂ nanoparticles" J. Am. Chem. Soc. 134 : 6575-6578.
- [135] Zhu W., Low T., Lee Y. H., Wang H., Farmer D. B., Kong J., Xia F. and Avouris P. (2014) "Electronic transport and device prospects of monolayer molybdenum disulfide grown by chemical vapour deposition" Nature comm. 1-8.
- [136] Yu C., Wenjing Z., Jing-Kai H., Keng-Ku L., Yi-Hsien L., Chi-Te L., Chih-Wei C. and Lain-Jong L. (2012) "Wafer-scale MoS₂ thin layers prepared by MoO₃ sulfurization" Nanoscale 2012.

- [137] Shi Y., Zhou W., Lu A. Y., Fang W., Lee Y., Hsu A. L., Kim S. M., Kim K. K., Yang H. Y., Li L., Idrobo J., and Kong J. (2012) "Van der waals epitaxy of MoS₂ layers using grapheme as growth templates" *Nano Lett.* 12: 2784-2791.
- [138] Etzkorn J., Helen A., Therese., Rocker F., Zink N., Kolb U., and Tremel W. (2005) "Metal-organic chemical vapor deposition synthesis of hollow inorganic-fullerene-type MoS₂ and MoSe₂ nanoparticles" *Adv. Mater.* 17: 2372-2375.
- [139] Pu J., Yomogida Y., Liu K., Li L., Iwasa Y. and Takenobu T. (2012) "Highly flexible MoS₂ thin-film transistors with ion gel dielectrics" *Nano Lett.* 12: 4013-4017.
- [140] Dominik L. and Andras K. (2012) "Breakdown of high-performance monolayer MoS₂ transistors" *ACS Nano.* 6:10070-10075.
- [141] Xiao J., Choi D., Cosimbescu L., Koech P., Liu J., and Lemmon J. P. (2010) "Exfoliated MoS₂ nanocomposite as an anode material for lithium ion batteries" *Chem. Mater.* 22: 4522-4524.
- [142] Maja R., Ales M., Zora S., Adolf J., Miran C., Jure D., Pierre S., Francis L. and Dragan Mihailovic. (2001) "Self-assembly of subnanometer-diameter single-wall MoS₂ nanotubes" *Sci.* 292: 479-481.
- [143] Splendiani A., Sun L., Zhang Y., Li T., Kim J., Chim C., Galli G. and Wang F. (2010) "Emerging photoluminescence in monolayer MoS₂" *Nano Lett.* 10:1271–1275.
- [144] Kirmayer S., Aharon E., Dovgolevsky E., Kalina M. and Frey G. I. *(2007) "Self-assembled lamellar MoS₂, SnS₂ and SiO₂ semiconducting polymer nanocomposites" *Phil. Trans. R. Soc. A.* 365: 1489–1508.
- [145] Rapoport L., Fleischer N. and Tenne R. (2005) "Applications of WS₂ (MoS₂) inorganic nanotubes and fullerene-like nanoparticles for solid lubrication and for structural nanocomposites" *J. Mater. Chem.* 15: 1782–1788.
- [146] Lauritsen J. V., Bollinger M. V., Laegsgaard E., Jacobsen K. W., Nørskov J. K., Clausen B. S., Topsøe H. and Besenbacher F. (2004) "Atomic-scale insight into structure and morphology changes of MoS₂ nanoclusters in hydrotreating catalysts" *J. Cata.* 221: 510–522.
- [147] Roy P. and Srivastava S. K. (2006) "Chemical bath deposition of MoS₂ thin film using ammonium tetrathiomolybdate as a single source for molybdenum and sulphur" *Thin Solid Films* 496: 293 – 298.
- [148] Jaramillo T. F., Jørgensen K. P., Bonde J., Nielsen J. H., Horch S., Chorkendorff I. (2007) "Identification of active edge sites for electrochemical H₂ evolution from MoS₂ nanocatalysts" *Science* 317: 100-102.

- [149] Nagaraju G., Tharamani C. N., Chandrappa G. T. and Livage J. (2007) "Hydrothermal synthesis of amorphous MoS₂ nanofiber bundles via acidification of ammonium heptamolybdate tetrahydrate" *Nanoscale Res. Lett.* 2:461–468.
- [150] Xiong Y., Xie Y., Li Z., Li X. and Zhang R. (2003) "Micelle-assisted fabrication of necklace-shaped assembly of inorganic fullerene-like molybdenum disulfide nanospheres" *Chem. Phys. Lett.* 382:180–185.
- [151] Santillo G., Deorsola F. A., Bensaid S., Russo N. and Fino D. (2012) "MoS₂ nanoparticle precipitation in turbulent micromixers" *Chem. Engg. J.* 1-7.
- [152] Li Q., Newberg J. T., Walter E. C., Hemminger J. C. and Penner R. M. (2004) "Polycrystalline molybdenum disulfide (2H-MoS₂) nano and microribbons by electrochemical/chemical synthesis" *Nano Lett.* 4: 277-281.
- [153] Skrabalak S. E. and Suslick K. S. (2005) "Porous MoS₂ synthesized by ultrasonic spray pyrolysis" *J. Am. Chem. Soc.* 127: 9990-9991.
- [154] Wu Z., Wang D. and Sun A. (2010) "Preparation of MoS₂ by a novel mechanochemical method" *Journal of Alloys and Compounds* 492: L5–L7.
- [155] Wu Z., Wang D. and Sun A. (2010) "Preparation of MoS₂ nanoflakes by a novel mechanical activation method" *J. Cryst. Growth* 312: 340–343.
- [156] Yitzhak M., Moshe H., Aharon G. and Gary H. (1999) "Room temperature sonochemical synthesis of molybdenum sulfide fullerene-like nanoparticles" *Adv. Mater.* 11: 1010-1013.
- [157] Mdeleleni M. M., Hyeon T. and Suslick K. S. (1998) "Sonochemical synthesis of nanostructured molybdenum sulfide" *J. Am. Chem. Soc.* 120: 6189-6190.
- [158] Chen J., Li S., Xub Q. and Tanakab K. (2002) "Synthesis of open-ended MoS₂ nanotubes and the application as the catalyst of methanation" *Chem. Com.* 1722–1723.
- [159] Lavayen V., Mirabal N., O'Dwyer C., Santa Ana M. A., Benavente E., Torres C. M. S. and González G. (2007) "The formation of nanotubes and nanocoils of molybdenum disulphide" *Appl. Surf. Sci.* 253: 5185–5190.
- [160] Friedel C. and Crafts J. M. (1888) "Sur une nouvelle méthode générale de synthèse des combinaisons aromatiques (deuxième mémoire)." *Ann. Chim. Phys.* 6 :433–472.
- [161] Edmonds J. T. and Hill H. W. (1967) "Production of polymers from aromatic Compounds" US Patent 3: 354:129, assigned to Phillips Petroleum Co. (Bartlesville, OK) 11-21.
- [162] "Commercial Plastics. polyethylene polyethylene is probably the polymer you see most in daily life. Polyethylene is the most popular plastic in the world." <http://slideplayer.com/slide/6233976/>

-
- [163] Cohen Y. and Aizenshtat Z. (1993) "Isothermal fluidized-bed studies on the kinetics and pyro-products of linear and branched poly(p-phenylene sulfide) and proposed mechanisms." J. Anal. Appl. Pyrolysis 27(2):131–143.
- [164] Das P. K., DesLauriers P. J., Fahey D. R., Wood F. K. and Cornforth F. J. (1995) "Photostabilization of poly (p-phenylene sulfide)." Polym. Degrad. Stabil. 48: 1–10.
- [165] Das A. P. K., DesLauriers P. J., Fahey D. R., Wood F. K. and Cornforth F. J. (1995) "Photodegradation and photostabilization of poly(p-phenylene sulfide). Part 2. UV induced physicochemical changes." Polym. Degrad. Stabil. 48:11–23.
- [166] Lábár J. L. (2002) "Introduction to electron microscopes: electron optics, interactions and signals".
- [167] Wang Z. L. (2003) "Characterization of nanophase materials" first Ed. Wiley-VCH, Verlag GMBH.
- [168] Kulkarni S. K. (2015) "Nanotechnology: principles and practices" Third Edition. Co-published by Springer International Publishing, ISBN 978-3-319-09170-9 ISBN 978-3-319-09171-6 (eBook).
- [169] Cullity B. D. (1978) "Elements of X-ray diffraction" 2nd Ed., Addison-Wesley.
- [170] Bowen D. K. and Brian K. T. (1998). Taylor & Francis, Ltd.
- [171] Glatter O. and Kratky O. (1982) "Small Angle X-ray Scattering" Academic Press.
- [172] https://en.wikipedia.org/wiki/Wide-angle_X-ray_scattering
- [173] Banwell C. N. and McCash E. M. (2002) "Fundamentals of molecular spectroscopy" Tata McGraw-Hill Publishing Company Limited, New Delhi.
- [174] http://en.wikipedia.org/wiki/Raman_spectroscopy
- [175] Guozhong C. (2004) "Nanostructures and nanomaterials, synthesis, properties and applications" Imperials College Press.